Anat Embryol (1991) 183:427–454

Anatomy
and Embryology

Distribution and targets of the cartwheel cell axon in the dorsal cochlear nucleus of the guinea pig

Albert S. Berrebi and Enrico Mugnaini

Laboratory of Neuromorphology, University of Connecticut, Storrs, CT 06269-4154, USA

Accepted January 11, 1991

Summary. This investigation attempted to determine the mode of distribution and synaptic targets of the cartwheel cell axon in the guinea pig dorsal cochlear nucleus (DCoN). Antiserum against PEP-19, a putative calcium-binding neuropeptide, was employed at the light and electron microscopic levels. We show that in the hindbrain of the guinea pig, cerebellar Purkinje cells and DCoN cartwheel cells are the most densely immunoreactive neurons. The PEP-19 immunoreaction product is localized to all neuronal compartments of these cells. Primary targets of cartwheel cell axons are the DCoN pyramidal cells, the large efferent neurons of layer 2. These neurons receive numerous immunoreactive synaptic boutons on their cell bodies and apical and basal dendritic arbors. A PEP-19-immunoreactive axonal plexus, largely formed by cartwheel cell axons, highlights layer 3, co-extensively with the basal arbors of pyramidal cells. This plexus is oriented predominantly in the transstrial plane of the DCoN, in parallel with the sheet-like basal dendritic arbor of pyramidal neurons and with the isofrequency bands of primary cochlear nerve fibers. PEP-19-positive boutons contain pleomorphic synaptic vesicles and form symmetric synaptic junctions, indicative of inhibitory innervation. In addition, immunoreactive boutons, similar to those synapsing on pyramidal neurons, were observed on the cell bodies and main dendritic trunks of cartwheel neurons, indicating a system of recurrent collaterals. Furthermore, a small number of PEP-19-positive axons of unknown origin reach the caudal rim of the posteroventral cochlear nucleus. Within the territory of distribution of the cartwheel cell axon are the dendrites of at least two other types of DCoN neuron, the vertical cells of Lorente de Nó and the giant cells. These neurons may represent additional targets of the cartwheel cell axon, but this remains to be ascertained with specific methods. Our data demonstrate that the cartwheel neurons modulate the activity of pyramidal neurons and, therefore, play a key role in shaping the output of the DCoN superficial layers.

Offprint requests to: A.S. Berrebi

Key words: Auditory brainstem – Immunoelectron microscopy – PEP-19

Introduction

Knowledge of the intrinsic organization of individual brain regions is extremely helpful for the understanding of their specific functions and extends our insight of the repertoire of biological neural microcircuits. This information is particularly compelling for first-order centers of sensory processing, where input parameters are better understood.

The dorsal cochlear nucleus (DCoN), or acoustic tubercle, has been much less studied than the ventral cochlear nucleus (VCoN), although they are both innervated by the acoustic, or cochlear, division of the VIIIth cranial nerve. In both regions, the cochlear nerve projections are ordered in a distinct cochleotopic (or tonotopic) array. Unlike the VCoN, the DCoN of most non-primate mammals is distinctly layered. Whereas in small rodents, such as mouse and rat, one can distinguish two superficial layers and a deep region, in cat four distinct layers and a central nucleus have been identified (reviewed by Lorente de Nó 1981; Blackstad et al. 1984). In guinea pig, the two superficial layers are very distinct, the layer 3–4 border is less clearly marked in standard histological sections, and a central nucleus is not distinguishable (Hackney et al. 1990). Layer 1 of the DCoN, the molecular layer, is innervated by a myriad of thin and varicose parallel fibers, the axons of granule neurons, whose parent cell bodies are situated in both the DCoN and VCoN. In most non-primate mammals, layers 1 and 2 contain at least five types of neuron, classified as pyramidal (or fusiform), granule, Golgi, stellate and cartwheel cells (Mugnaini et al. 1980a, b; Blackstad et al. 1984; Wouterlood et al. 1984; Wouterlood and Mugnaini 1984), the last four of which form an intrinsic neuronal microcircuit resembling that of the cerebellar cortex. The cartwheel cells have been proposed to represent

the counterpart of the Purkinje cells (Mugnaini 1985; Mugnaini and Morgan 1987; Berrebi and Mugnaini 1988b; Berrebi et al. 1990). In the guinea pig DCoN, most cartwheel cells are situated at the border between layers 1 and 2, and most of the granule cells are clustered between the pyramidal cell bodies, which traditionally characterize layer 2. The pyramidal cells, which project to the central nucleus of the contralateral inferior colliculus, represent the efferent neurons of the two superficial DCoN layers. Most pyramidal cells are provided with densely branched apical dendrites extending into the molecular layer and sparsely branched basal dendrites extending into the deep region (Blackstad et al. 1984). By definition, the extent of the basal dendritic fields of pyramidal neurons defines the third layer. In guinea pig, a narrow layer 3 is distinguishable in silver preparations following degeneration of the cochlear fibers which innervate the basal arbors of pyramidal cells (Osen 1988; Hackney et al. 1990). Because of the accentuated curvature of the DCoN, layer 4 is only present in the center of the nucleus where it is rather prominent.

Immunocytochemical and electron microscopic studies have indicated that cartwheel neurons, which are labelled by antisera to GAD (Mugnaini 1985), GABA and glycine (reviewed by Osen et al. 1990), are presumably inhibitory and may serve to modulate the activity of pyramidal cells (Mugnaini 1985; Caspary et al. 1987; Caspary 1990). However, several factors have hampered the effort to identify with precision the mode of distribution and the synaptic target(s) of this cell class. The cartwheel axon develops a thin myelin sheath at a short distance from the cell soma and could not be revealed by the combined Golgi rapid-electron microscopy method (Wouterlood and Mugnaini 1984). Furthermore, antiserum to cerebellin, a polypeptide expressed by the entire populations of cerebellar Purkinje cells and DCoN cartwheel cells, reveals somatal and dendritic neuronal compartments, but not axons (Mugnaini and Morgan 1987; Mugnaini et al. 1988).

We have recently reported that PEP-19, a putative calcium-binding protein (Ziai et al. 1986, 1988), is expressed by the entire populations of cerebellar Purkinje neurons and DCoN cartwheel neurons in mouse (Mugnaini et al. 1987), including their entire dendritic and axonal arborizations. In the murine DCoN, all other cell classes were either completely immunonegative or only faintly immunopositive. Distinctly immunostained neurons, however, were scattered in the VCoN and in other regions of the acoustic brainstem. PEP-19-positive axons derived from these centers may innervate the DCoN and hinder the identification of cartwheel cell axons. Preliminary experiments (Berrebi and Mugnaini 1988a) indicated that PEP-19 expression is especially selective in the guinea pig compared to other species; cerebellar Purkinje cells and DCoN cartwheel cells are the only densely immunostained neurons in the hindbrain. Thus, in this study we describe the localization of PEP-19-like immunoreactivity in the guinea pig DCoN, taking advantage of both the more restricted expression of this peptide and the particularly distinct lamination of the superficial DCoN in this animal. Our main goal was to uncover the mode of distribution and targets of the cartwheel cell axon.

Materials and methods

Adult guinea pigs (ages 2–6 months, $n=30$), derived from a closed colony at the National Institutes of Health (Bethesda, Md.), were used in these studies. The animals were deeply anesthetized by intramuscular injection of a 3:4 mixture of Rompun (Haver) and Ketaset (Aveco Co.) (0.12 ml/100 g body weight), and perfused through the ascending aorta as previously specified (Friedrich and Mugnaini 1981).

Fixation and tissue sectioning. Briefly, fixation for light microscopy was performed as follows. Perfusion was initiated with a 0.9% NaCl vascular rinse, followed by 1 l of a zinc-aldehyde fixative (Mugnaini and Dahl 1983) consisting of 4% commercial formaldehyde and 0.5% zinc dichromate (K and K Laboratories) in 0.75% NaCl (pH 4.8). Perfusates were delivered at room temperature via gravity flow (delivery pressure = 115 cm H_2O). Brainstems and cerebella were dissected from the cranium and cryoprotected in 30% sucrose in 0.9% NaCl for 2–3 days, and then sectioned on a freezing microtome at a thickness of 25 μm in either the coronal, sagittal or horizontal plane.

Guinea pigs to be used for electron microscopy were perfused first with a calcium-free variant of the Ringer solution, saturated with 95% CO_2 and 5% O_2 to pH 7.2, then by a fixative composed of 4% freshly depolymerized paraformaldehyde and 0.125% glutaraldehyde (TAAB, Marivac Ltd.) in 0.12 M sodium phosphate buffer (pH 7.3), followed by 4% paraformaldehyde in the same buffer. The brainstems were sectioned on a vibrating blade microtome at a thickness of 35 μm, and collected in cold TRIS-buffered saline (TBS, 295 mosmol).

Immunocytochemical protocol. For light microscopy, floating sections were reacted using the single peroxidase/antiperoxidase (PAP) procedure (Sternberger 1979) as follows: incubation for 1 h in 5% normal donkey serum and 0.5% Triton X-100; 40 h at 4° C in the polyclonal rabbit anti-PEP-19 antiserum P2 (previously characterized; see Ziai et al. 1986, 1988; Mugnaini et al. 1987) diluted 1:1000, with 1% normal donkey serum and 0.1% Triton X-100; 30 min in goat anti-rabbit antiserum, diluted 1:100; 30 min in rabbit-PAP, diluted 1:100; 15–30 min in 0.05% diaminobenzidine (DAB) and 0.01% H_2O_2. All immunoreagents were diluted in 0.5 M TRIS-HCl buffer, pH 7.6, which was also used as the rinsing solution between each step of the immunoreaction. Most sections were wet-mounted onto glass slides from phosphate-buffered saline (PBS) and coverslipped with a glycerol/phosphate mounting medium, or dry mounted from a gelatin/alcohol solution and coverslipped with Accumount-60 (Baxter Scientific). Some sections were osmicated, dehydrated, flat-embedded in Epon 812 (LKB) (as specified below), and cut at a thickness of 2 μm for examination in the light microscope.

The immunoelectron microscopy protocol was as described above, with the following variants: the Triton X-100 was eliminated, TRIS-buffered saline (TBS) was used as the diluent, and incubation in primary antiserum took place overnight only. After immunoreaction, sections were rinsed in 0.12 M sodium phosphate buffer (pH 7.3), post-fixed in 2% buffered osmium tetroxide for 1 h, rinsed thoroughly in distilled water, stained in 2% aqueous uranyl acetate, rinsed in distilled water, dehydrated in graded ethanols and propylene oxide, and flat-embedded in Epon 812. Series of ultrathin sections were collected on Formvar-coated single-hole grids, stained for 3 min with lead citrate and examined in a Zeiss EM-10 electron microscope operated at 80 kV.

As a control, some sections were incubated in normal rabbit serum instead of the PEP-19 antiserum. These were completely free of immunoreaction product (not illustrated).

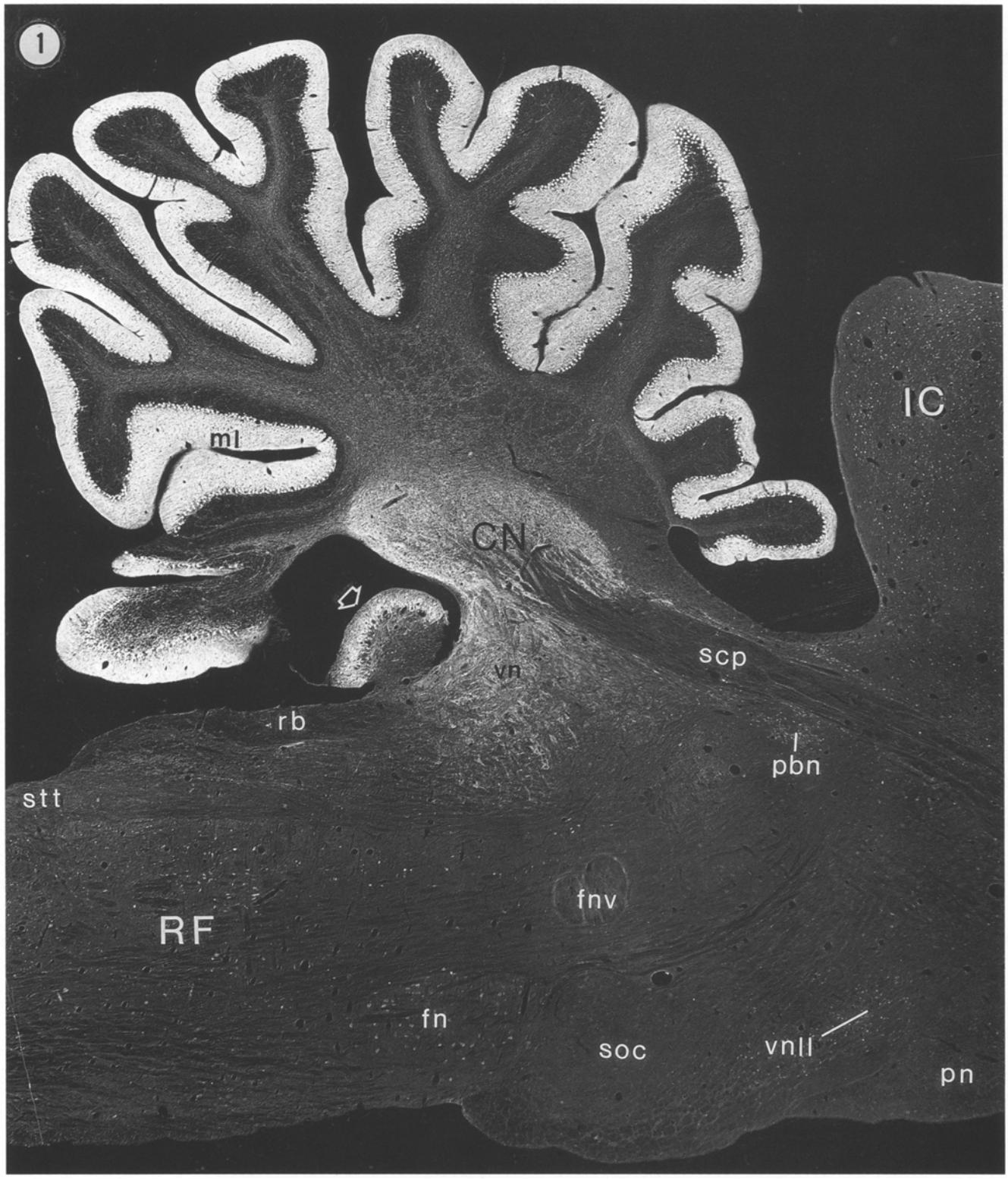

Fig. 1. This negatively printed microphotograph of a parasagittal section demonstrates the restricted PEP-19-like immunoreactivity in the guinea pig hindbrain. Immunostaining is densest in the cerebellar cortex, deep cerebellar nuclei (*CN*), vestibular nuclei (*vn*) and the dorsal cochlear nucleus (*open arrow*). *fn*, Facial nucleus; *fnv*, facial nerve; *IC*, inferior colliculus; *ml*, molecular layer of cerebellum; *pbn*, parabrachial nucleus; *pn*, pons nuclei; *rb*, restiform body; *RF*, reticular formation; *scp*, superior cerebellar peduncle; *soc*, superior olivary complex; *stt*, spinal trigeminal tract; *vnll*, ventral nucleus of the lateral lemniscus. ×18

Results

Light microscopy

Figure 1 shows the restricted distribution of PEP-19-like immunoreactivity in the hindbrain. The cerebellar cortex is densely immunolabelled, due to the abundance of antigen within the somata and dendritic processes of the Purkinje cells (Fig. 2). Purkinje axons are also visualized; they course through the granular layer, aggregate into bundles in the folial white matter, and proceed toward the deep cerebellar and vestibular nuclei (Figs. 1, 2). These nuclei appear heavily innervated by immunoreactive axon terminals. Besides the cerebellum, the DCoN is the only other hindbrain region richly provided with densely PEP-19 immunoreactive cell bodies, dendrites and axons (Figs. 1, 3). Immunostained neurons are found in the inferior colliculus (Fig. 1), the sagulum, the lemniscal nuclei and the ventral nucleus of the trapezoid body, but these centers contain antigen mostly in cell bodies and proximal dendrites. Specific immunostaining is absent or below detection level in the remaining portions of the entire superior olivary complex (Fig. 1). The region occupied by the dorsal and intermediate acoustic striae contains weakly immunoreactive fibers, but these belong, at least for the most part, to the efferent neurons of the DCoN (see below). The descending fiber tract of Lorente de Nó (Fig. 4A) contains only a few immunostained fibers. The primary cochlear fibers in the nerve root, the ventrotubercular tract, the trapezoid body (Figs. 3A, 10C) and the posteroventral cochlear nucleus (PVCoN) (Figs. 3, 10) are hardly stained at all; only faint staining of cell bodies is seen in the spherical cell area of the anteroventral cochlear nucleus (AVCoN) (Fig. 3). In some sections (Fig. 3A), the neuropil of this area shows a diffuse background, but is devoid of distinctly immunostained processes. Thus, no nerve cell population whose axonal pathway represents a potential source of afferents to the DCoN is markedly labelled. This mode of distribution of the immunoreaction product supports the notion that in the DCoN, as in the cerebellum, PEP-19 immunoreactive elements are intrinsic, at least for the most part. Other systems not included in the acoustic brainstem show moderate-to-distinct immunoreactivity: the principal neurons throughout the inferior olivary complex are weakly stained, the vestibular ganglion cells are also immunolabelled but show great variability in staining intensity, the primary vestibular fibers and some fibers in the restiform body are moderately immunostained, and the pyramidal tract and spinal tract of the trigeminal nerve are well labelled, as are some cell bodies and fibers in the reticular formation. Some of the above-mentioned centers and tracts, which are beyond the scope of this investigation, appear in Figs. 1, 3, 9, 10 and 11.

Figure 3 illustrates, in two planes of section, the light

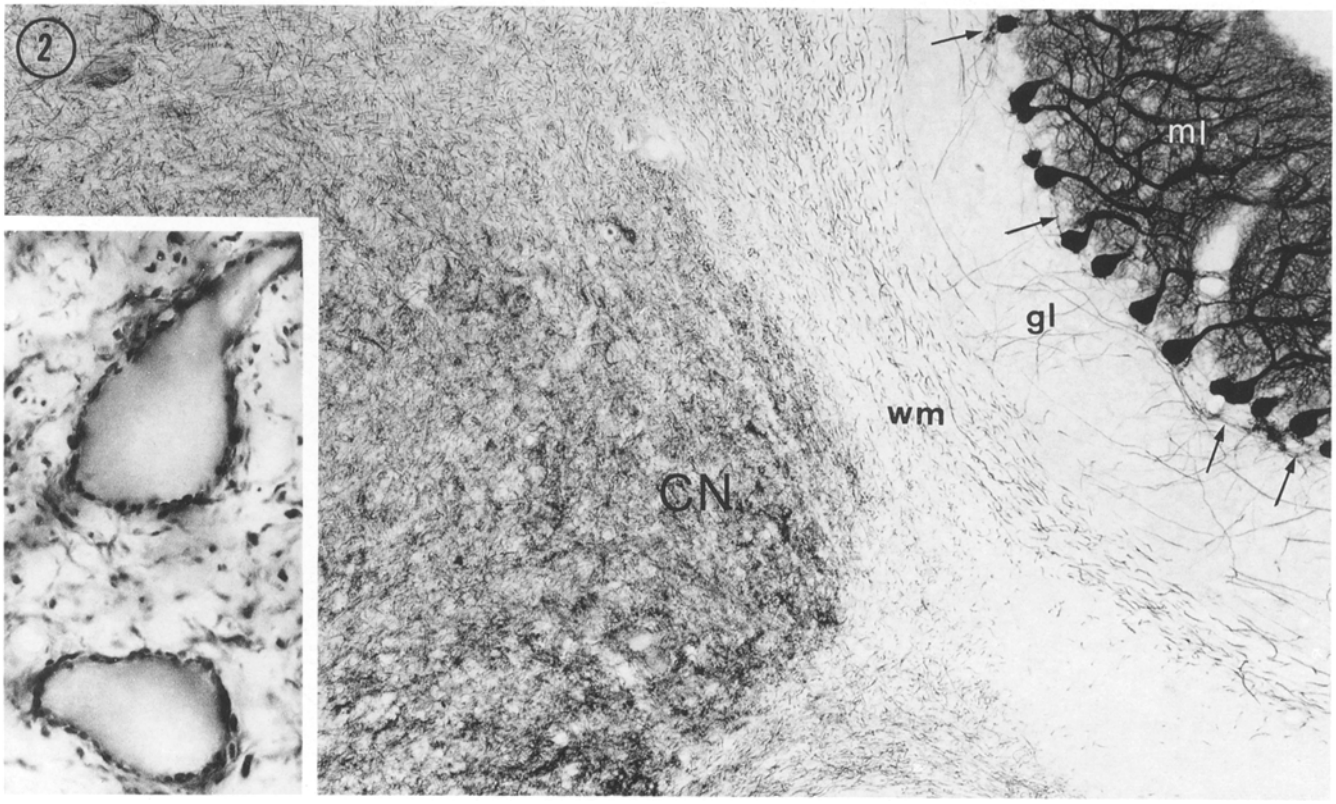

Fig. 2. Cerebellar Purkinje cell bodies, their dendrites in the molecular layer (*ml*) and axons in the granular layer (*gl*) strongly express the PEP-19 antigen. Purkinje axons can also be seen in the folial white matter (*wm*) and their terminals innervate the deep cerebellar nuclei (*CN*). *Thin arrows* indicate Purkinje axon recurrent collaterals of the infraganglionic plexus. × 150. *Inset*: Densely stained Purkinje axon terminals surround large immunonegative neurons in the deep cerebellar nuclei. × 700

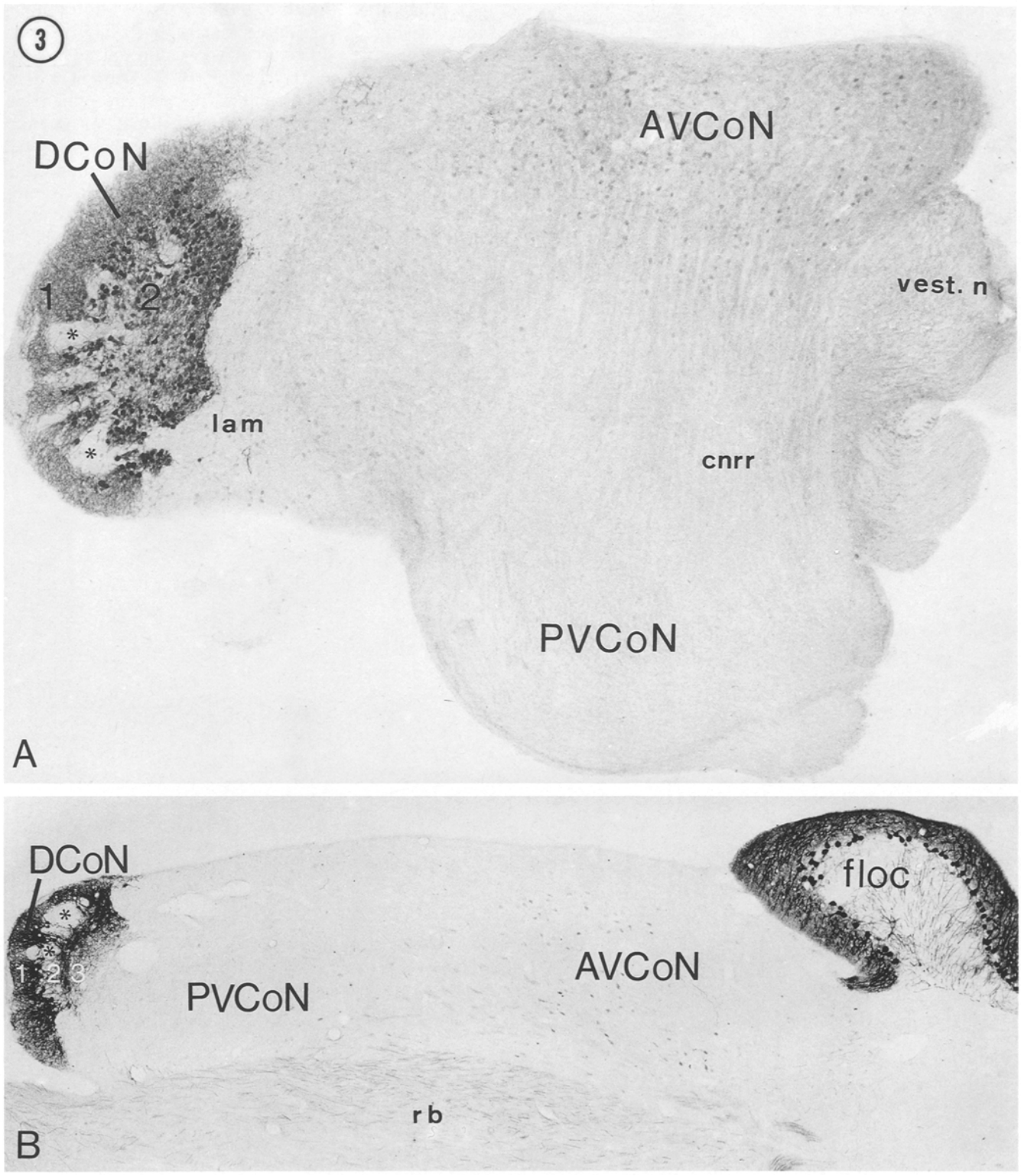

Fig. 3A, B. These light micrographs illustrate the cochlear nuclear complex in the parasagittal (**A**) and horizontal (**B**) planes of section. **A** Dense PEP-19 immunostaining in the cochlear nuclear complex is restricted to the dorsal cochlear nucleus (*DCoN*). At this lateral level, only layers 1 and 2 of the DCoN are included. Faint immunostaining in the spherical cell area of anteroventral cochlear nucleus (*AVCoN*) can be seen. *Asterisks* in the DCoN mark areas, void of immunoreaction product, which are occupied by granule cells. *PVCoN*, Posteroventral cochlear nucleus; *lam*, granule cell lamina; *cnrr*, cochlear nerve root region; *vest. n*, vestibular nerve root. ×50. **B** In this horizontal section, layers 1–3 of DCoN appear densely stained, except in the regions containing granule cell clusters (*asterisks*). The PVCoN is unstained; the AVCoN contains weakly immunoreactive nerve cell bodies. *floc*, Cerebellar flocculus; *rb*, restiform body. ×40

microscopic distribution of PEP-19 in the cochlear nuclear complex. The DCoN contains numerous immunoreactive neuronal cell bodies and processes, in marked contrast to the VCoN. DCoN layers 1 through 4 are clearly evident in Fig. 4, which illustrates the center of the nucleus in sagittal (Fig. 4A) and coronal (Fig. 4B) section. Numerous thin processes are present in layer 3, while these are much less frequent in layer 4.

In order to better familiarize the reader with the composition of the guinea pig DCoN, we have included a photomicrograph of a semi-thin (2 μm thick) section of the nucleus stained with toluidine blue, but not immunoreacted (Fig. 5). The molecular layer (layer 1) is covered by ependyma and contains few neuronal cell bodies. The border between layers 1 and 2 is demarcated by the medium-sized cell bodies of cartwheel neurons. Layer 2 contains large pyramidal cells and numerous granule cells, most of which are organized into clusters. There are numerous medium-sized cell bodies in layer 3, many of which represent the vertical cells of Lorente de Nó (1981). The limit between layers 3 and 4 cannot be clearly discerned in this preparation. Giant cells are

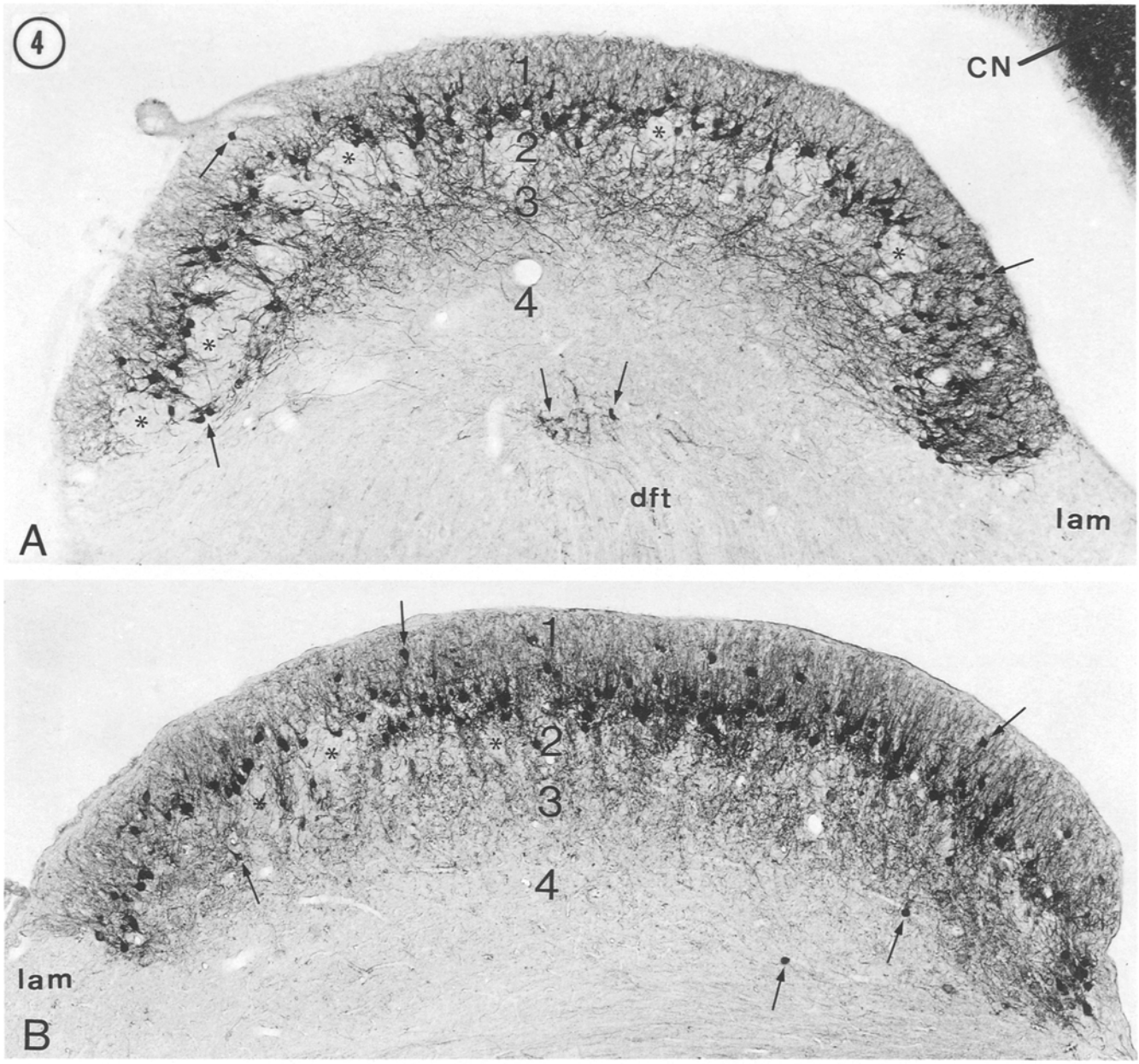

Fig. 4. **A** Parasagittal and **B** coronal sections of the DCoN show the distribution of PEP-19 immunoreactivity. In **A**, caudal is to the left; in **B** ventrolateral is to the left. The layers are indicated by Arabic numerals. Immunolabelled cartwheel cells are situated mostly at the border of layers 1 and 2. *Arrows* indicate displaced cartwheel neurons. A plexus of fine processes (**A**) and puncta (**B**) mark the position of layer 3. Fewer immunoreactive profiles are present in layer 4. The descending fiber tract of Lorente de Nó (*dft*) contains few immunostained fibers. *Asterisks* mark immunonegative granule cell clusters. *CN*, Cerebellar nuclei; *lam*, granule cell lamina. × 75

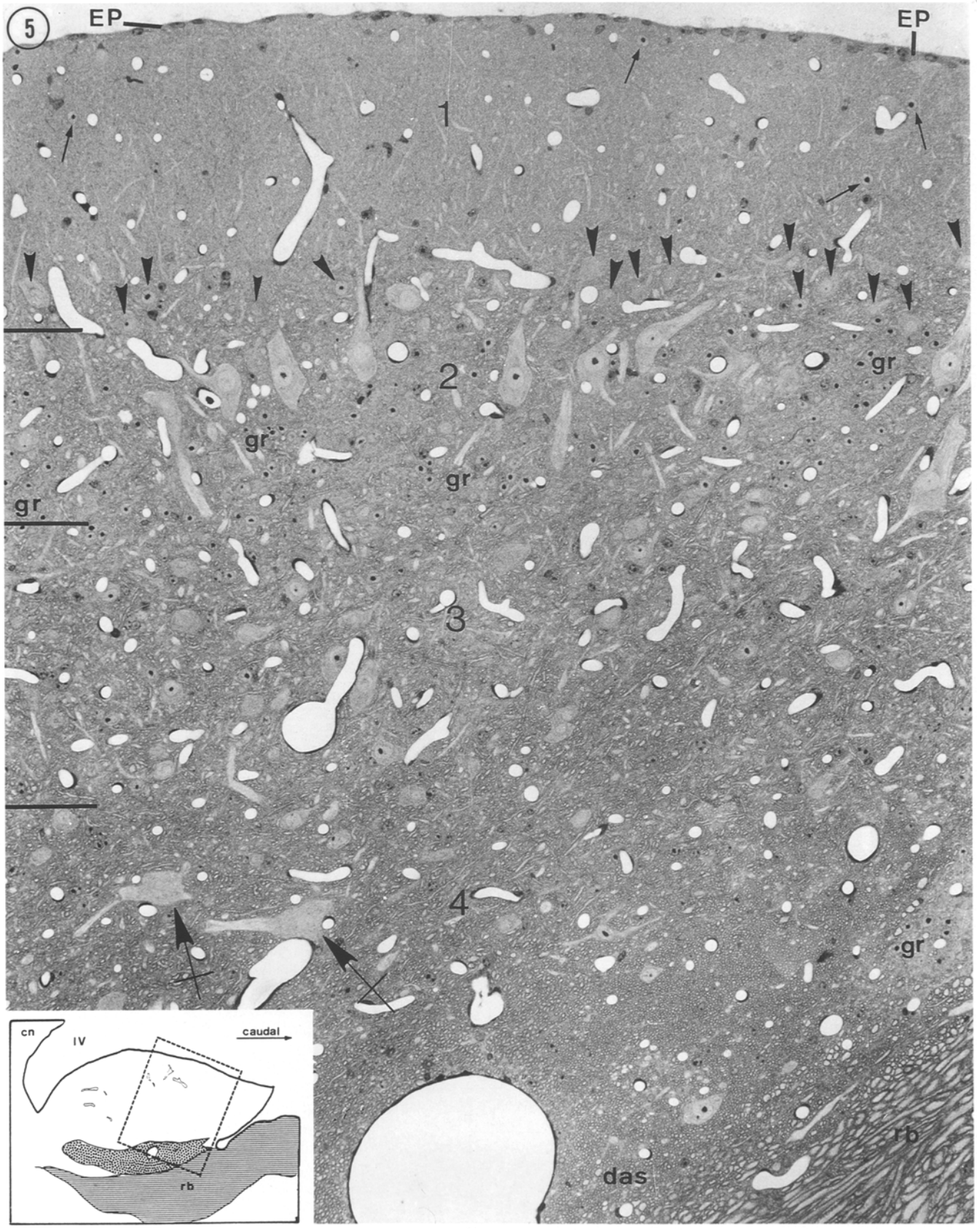

Fig. 5. Photomicrograph of a semithin (2 μm thick) transstrial section of the DCoN. This toluidine blue-stained slice of a resin-embedded, aldehyde-osmium-fixed tissue block, was not immunoreacted. Layers are indicated by Arabic numerals, and their approximate borders are shown by *solid lines* on the left hand side. *Inset* illustrates orientation of the photograph. Layer 1, which is covered by ependyma (*EP*) contains few neuronal cell bodies (*arrows*). *Arrowheads* indicate cartwheel neurons, some of which are sectioned through the nucleus. The large pyramidal cells in layer 2 are unlabelled. *Crossed arrows* point to giant cells in layer 4. *das*, Dorsal acoustic stria; *gr*, granule cell clusters; *rb*, restiform body. ×320. *Inset: cn*, cerebellar nuclei; *IV*, fourth ventricle; *rb*, restiform body

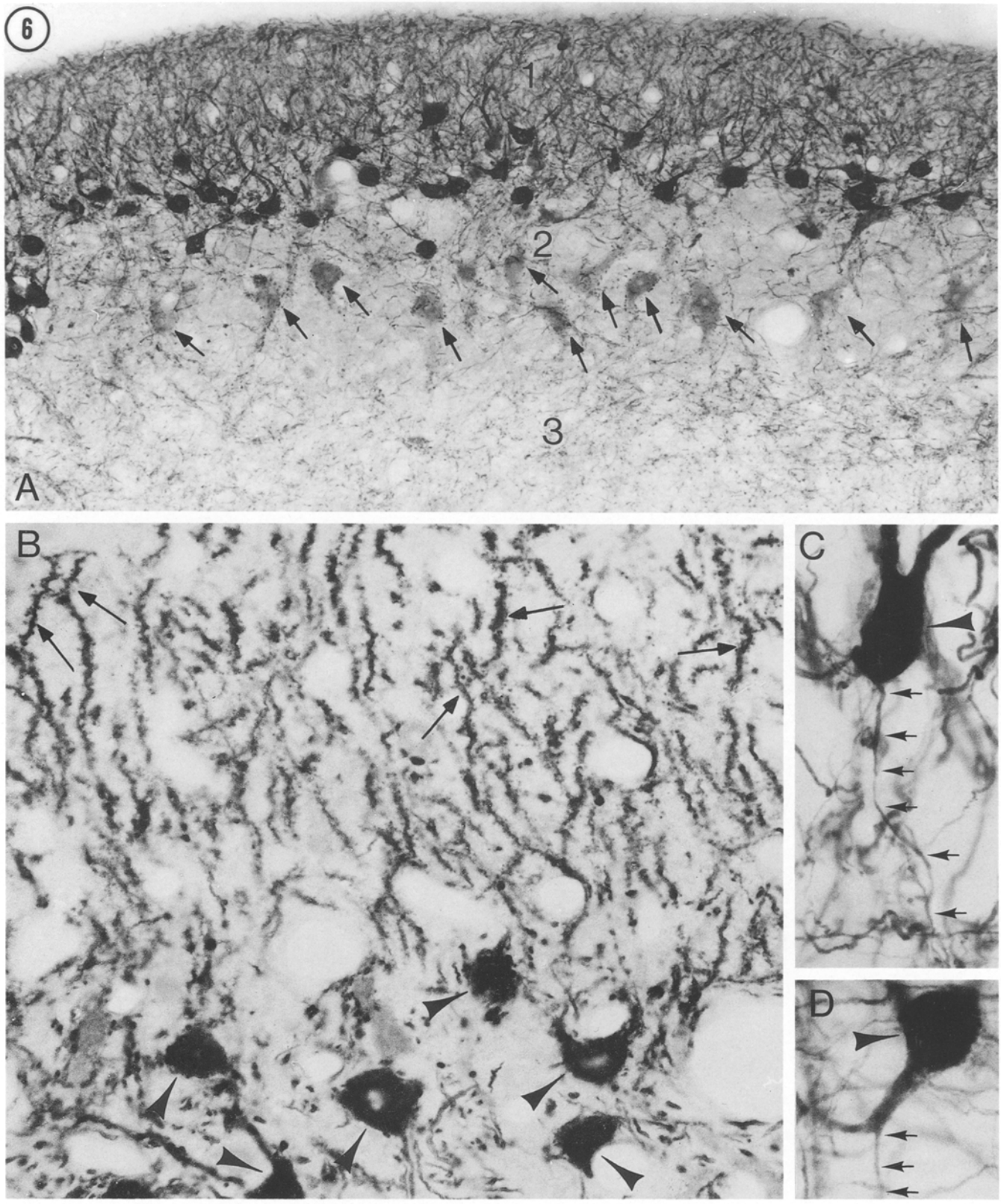

Fig. 6A–D. This micrograph shows the high density of cartwheel neurons and their dendrites in layer 1. It is also apparent that pyramidal cells (*arrows*), situated somewhat deeper in layer 2, are faintly immunostained by our antiserum. However, the staining reveals mostly the cell bodies and primary dendrites of these cells, which are larger and less numerous than cartwheel neurons. Layers are indicated by Arabic numerals. Parasagittal section. ×250. **B** This semithin (2 μm) section through the immunostained DCoN molecular layer reveals the high density of spiny dendrites (*arrows*) belonging to cartwheel neurons (*arrowheads*). ×820. **C** The immunostained axon (*arrows*) of this cartwheel neuron (*arrowhead*) emerges from its cell body. It can be followed to layer 3. ×880. **D** The axon (*arrows*) of this cartwheel neuron (*arrowhead*) emanates from a thick primary dendrite. ×880

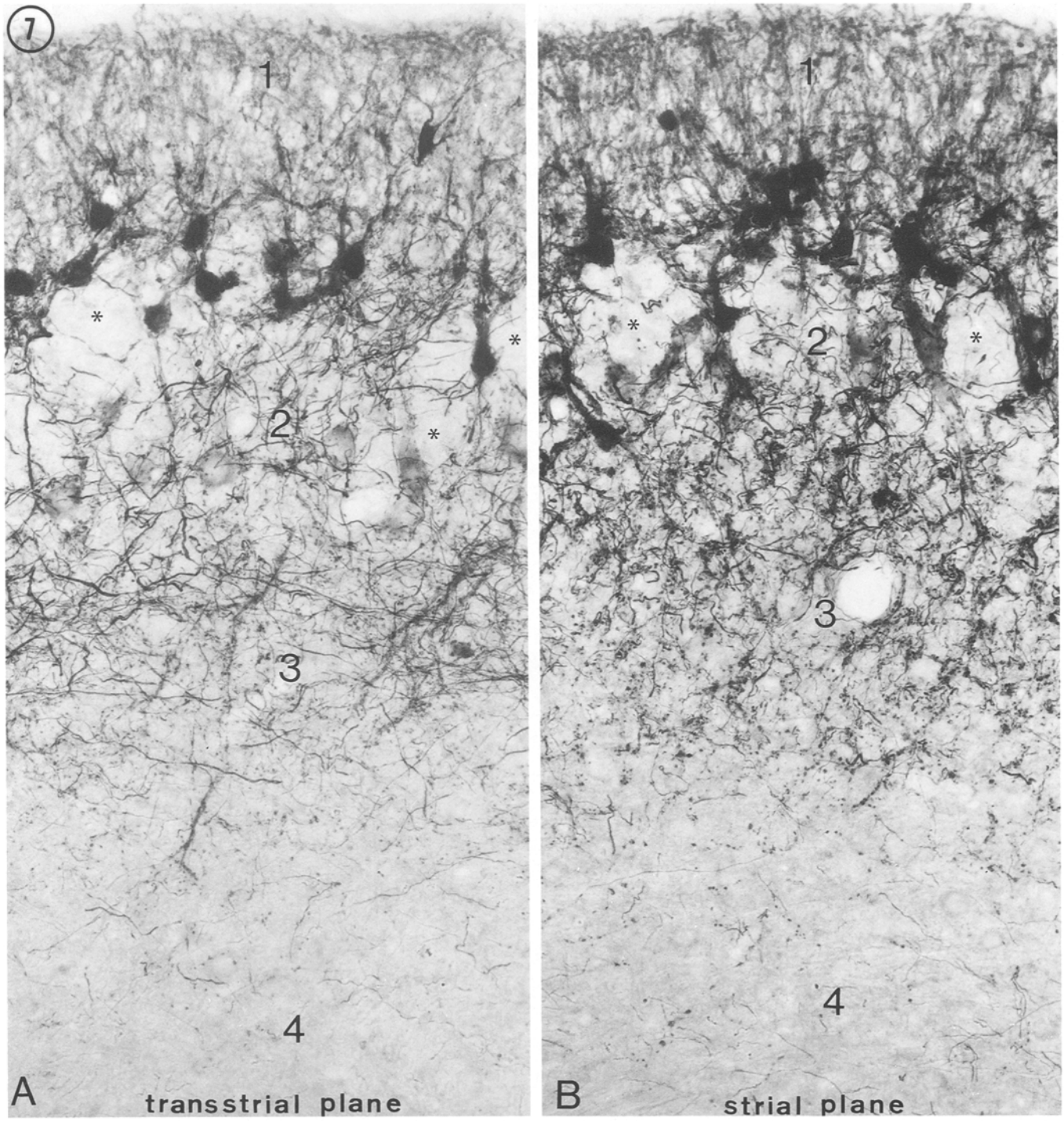

Fig. 7. A This parasagittal section shows the predominantly transstrial orientation of the cartwheel axonal plexus in layer 3. Most immunolabelled puncta are interpreted as boutons. *Asterisks* mark immunonegative granule cell clusters. ×280. **B** In this coronal section the cartwheel axons in layer 3 appear mostly as short fiber segments and punctate profiles, which are hardly distinguishable from axon terminals. *Asterisks* mark immunonegative granule cell clusters. ×280

seen in the deep region near the cross-sectioned dorsal acoustic stria (DAS). In the guinea pig, the course of the stria and the main axis of the DCoN are oriented nearly parallel to the coronal and horizontal planes of section (Hackney et al. 1990). This situation differs from that in the cat, where the stria and the main axis of the nucleus run at angles with the anatomical reference planes. Blackstad et al. (1984) introduced the terms 'strial' and 'transstrial' to denote the planes parallel and orthogonal to the main axis of the DCoN. Thus, in guinea pig, the strial and transstrial planes are roughly parallel to the coronal and sagittal planes, respectively.

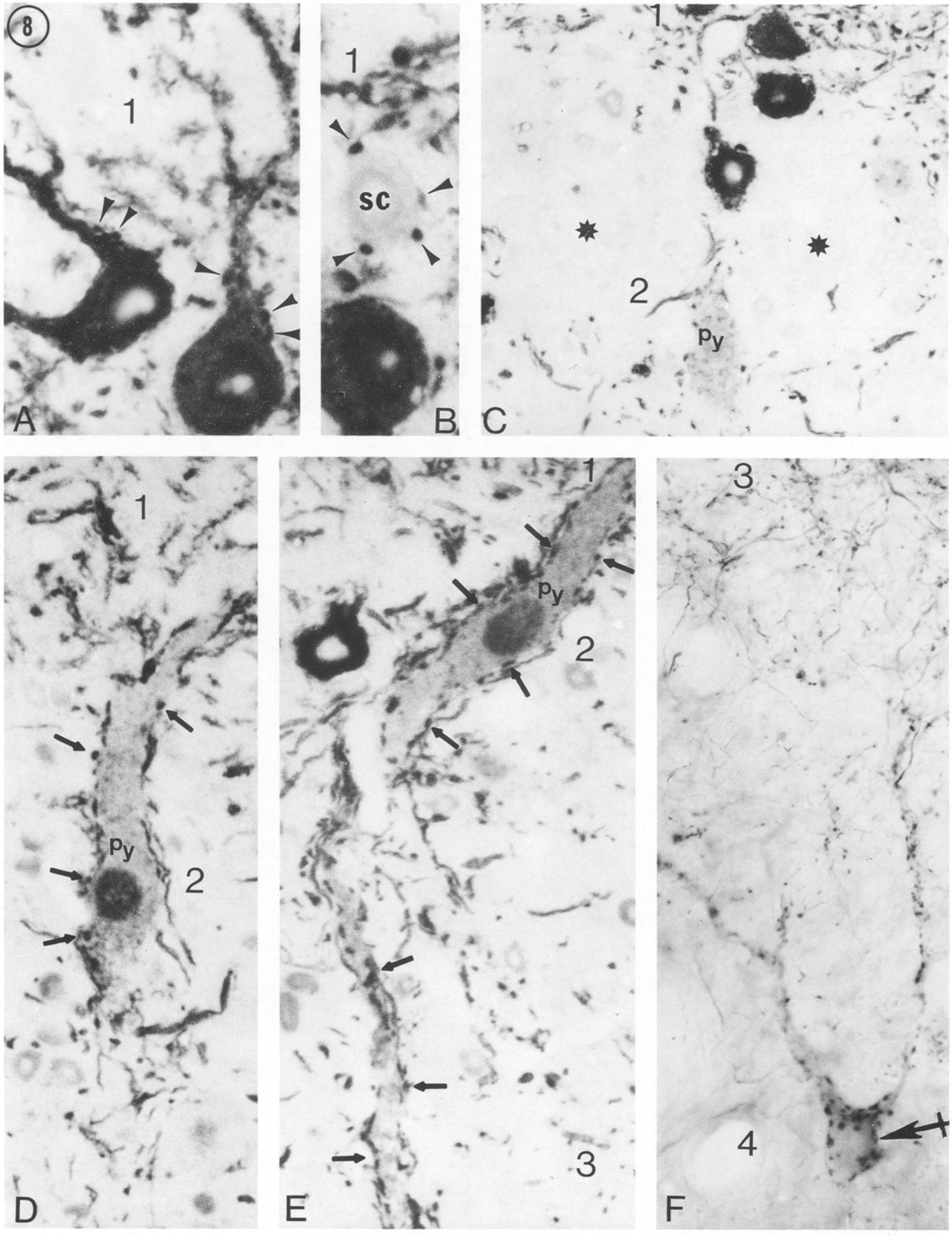
8
1
A
1
sc
B
1
2
py
C
1
py
2
D
1
py
2
3
E
3
4
F

At medium and high magnification (Figs. 4, 6), it is evident that the dense PEP-19-like immunoreactivity is largely localized to a population of medium-sized oval or rounded neurons (15–20 μm in average diameter), identified as cartwheel neurons by virtue of their distribution and morphological features established in Golgi sections (Hackney et al. 1990). Most of these densely stained cells are situated in a staggered array at the border between layers 1 and 2, but some of them also occur in adjacent areas of layers 1 and 2. The dendritic processes of the cartwheel neurons extend some branches into layer 2, but most of the branches are oriented radially and reach toward the ependymal lining. In coronal sections, the cartwheel cell dendrites appear more radially oriented than in sagittal sections. This suggests that the dendritic fields of individual cells are wider in the transstrial direction than in the strial direction. These dendrites occupy a substantial proportion of layer 1, which, consequently, appears densely immunostained (Fig. 6). The numerous spines of cartwheel cell dendrites are clearly revealed in semithin sections of immunoreacted slices (Fig. 6B). As already noted by Hackney et al. (1990), the cartwheel cell dendritic arbor in the guinea pig differs from that in the cat, which is tumbleweed shaped and also from that of the rat, which has curved dendrites but is more sparsely branched (Wouterlood and Mugnaini 1984). The cartwheel cell axon emanates from the cell body (Fig. 6C) or from a primary dendrite (Fig. 6 D), and it can often be followed to layer 2 or even layer 3. Layers 2 and 3 contain a high density of immunoreactive fibers and puncta (Fig. 7). These structures are interpreted as PEP-19-containing fibers and terminals, most of which presumably belong to the axonal plexus of cartwheel neurons (see below). Long immunoreactive fibers (Fig. 7A) are predominant in layer 3 when the DCoN is sectioned in the transstrial, or sagittal, plane. However, when viewed in the strial, or coronal, plane, shorter fiber segments and puncta prevail (Fig. 7B). Thus, the immunostained axonal plexus has a predominantly transstrial orientation. PEP-19-positive boutons in contact with the cell bodies and dendrites of cartwheel neurons are frequently observed (Fig. 8A). The immunostained plexus of layers 2 and 3, however, is mainly seen in close relation to the cell bodies and dendrites of pyramidal neurons (Figs. 6A, 7, 8D, E). Their fusiform somas measure 20–25 μm in short diameter and 26–34 μm in long diameter. The cell bodies and mainstem dendrites are barely immunostained above background, but they stand out nevertheless because they are studded with densely immunoreactive boutons (Figs. 6A, 8D, E). The peripheral branches of the apical dendritic arbor are usually not evident in the PEP-19 immunoreacted sections, while those of the basal arbor are outlined by numerous immunostained boutons. Fewer PEP-19-positive boutons are present in layer 4, which as a consequence appears much lighter (Fig. 7). It should be recalled that this layer is evident only in the central region of the DCoN because of the accentuated curvature of the nucleus (Hackney et al. 1990).

No other neuronal families in the DCoN superficial layers are stained by our antiserum. In fact, regions containing clusters of granule cells are completely void of immunoreaction product or contain only passing immunostained fibers, and are therefore quite conspicuous by virtue of their negativity (Figs. 3, 4A, 7, 8C). These clusters tend to be more prominent caudally and laterally than rostrally and medially. Overall, the granule cell bodies in layer 2 are more clustered in guinea pig than in rat and cat. The medium-sized vertical cells of layer 3 are immunonegative, and their cell bodies are not found in contact with PEP-19-positive boutons in immunoreacted sections counterstained with toluidine blue. We have observed small (9–10 μm in average diameter) immunonegative neurons in layer 1 (Fig. 8B), identified as stellate cell bodies, and scattered large (25 μm in average diameter) neurons in layer 4 (Fig. 8F) and along the stria, that are in contact with immunoreactive axon terminals. Some of these deep neurons are weakly immunostained, like the pyramidal cells, while others are definitely immunonegative. They may present ectopic pyramidal cells and a class of giant cells, respectively.

Besides the cartwheel neurons of the superficial DCoN layers, other densely immunostained neurons occur close to the dorsal acoustic stria in the deep DCoN. At this site the cells form an aggregate that differs in appearance, depending on the plane of section. In sagittal section the cell aggregate appears as a cluster (Figs. 4A, 11A), in coronal section as a thin band (Fig. 9A) and in horizontal section as an oblong cell group (Fig. 9C) that shifts in position as the plane of section progesses from dorsal to ventral (not illustrated). Other densely immunostained neurons are scattered in the granule cell lamina separating DCoN and VCoN (Fig. 9B), the superficial granule cell layer (Fig. 9D) and the medial border of VCoN, which includes the medial sheet of granule cells according to Mugnaini et al. (1980a, b) (Fig. 9E). By immunoelectron microscopic criteria (described below), these additional densely stained neurons were identified as cartwheel neurons. The number and distribution of cartwheel neurons situated outside the border region of layers 1 and 2 of DCoN vary greatly, even among animals of the same litter, and we therefore consider them ectopic elements. Thus, ectopic cartwheel neurons in the guinea pig are

Fig. 8. A–E Microphotographs from semithin (2 μm) sections of immunoreacted, plastic-embedded slices of DCoN. **F** An immunoreacted frozen section. Arabic numerals indicate the layers from which the detailed pictures were obtained. **A** PEP-19-positive axon terminals (*arrowheads*) contact the densely stained cell bodies and dendrites of cartwheel neurons. ×1900. **B** Four immunostained axon terminals (*arrowheads*) are closely apposed to a small immunonegative neuron in the molecular layer, presumably a stellate cell (*SC*). ×1900. **C** In layer 2, areas devoid of immunoreactive terminals and penetrated only by an occasional positive fiber contain clusters of immunonegative granule cells (*asterisks*). *py*, Pyramidal cell. ×800. **D–E** The weakly immunoreactive cell bodies (*py*) and apical and basal dendrites of pyramidal neurons are outlined by numerous immunostained axon terminals (*arrows*). ×925. **F** Unidentified large neuron (*crossed arrow*) in the deep DCoN region is studded with PEP-19-positive axon terminals. ×500

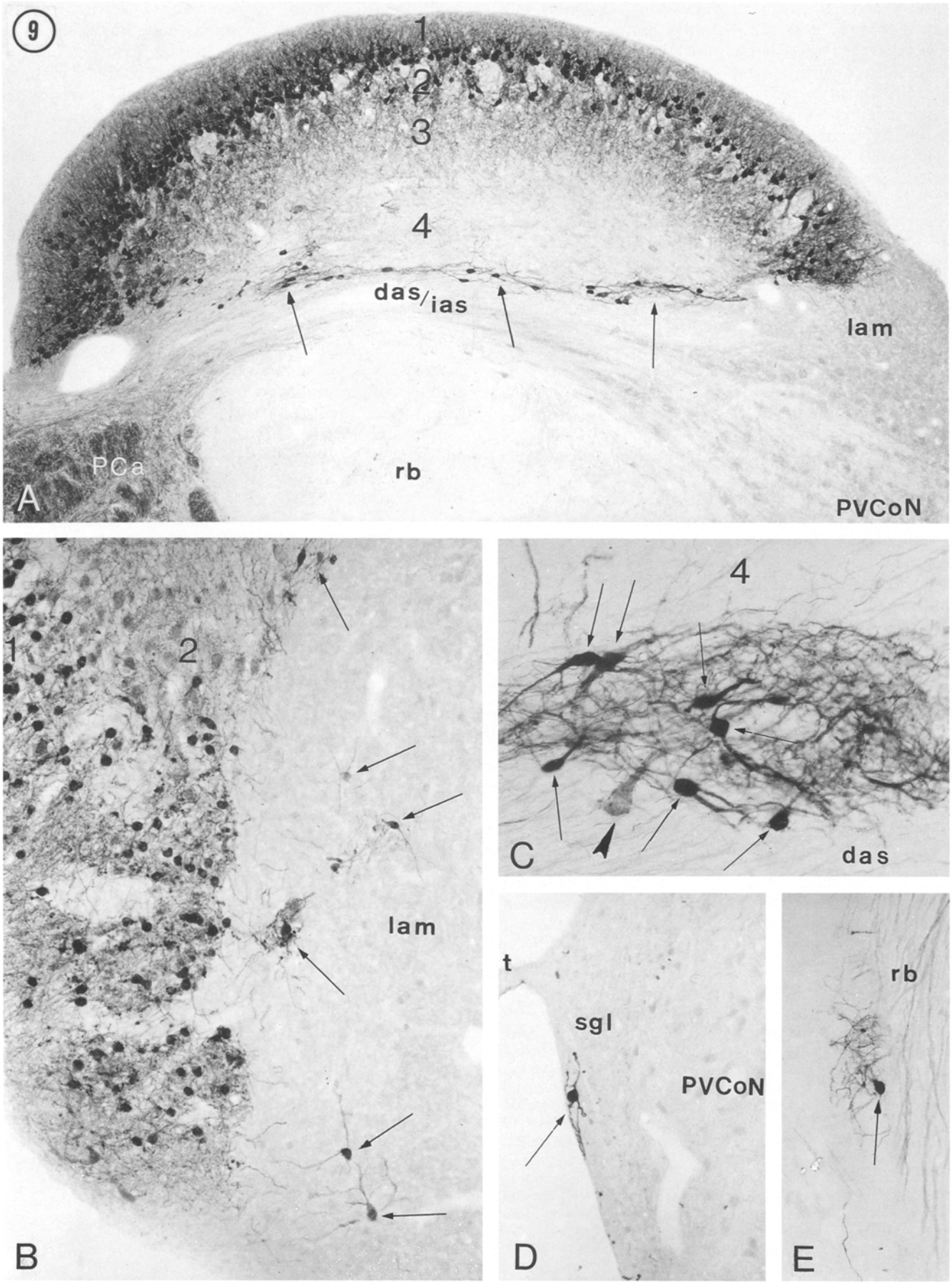
9
1
2
3
4
das/ias
lam
PCa
rb
A
PVCoN
1
2
lam
B
4
C
das
t
sgl
PVCoN
D
rb
E

distributed in all regions of the cochlear nuclei which contain granule cells. This feature has been described previously in rat (Mugnaini and Morgan 1987) and cat (Osen 1985). The guinea pig differs from rat and cat in having a greater number of ectopic cartwheel neurons in the deep DCoN. This may be related to the quasi-hemicylindrical shape of the nucleus in this species. This configuration creates a sort of invagination of the superficial layers at the perimeter of the DCoN. Cartwheel, and to a lesser extent also pyramidal neurons, by consequence, can extend along the stria from these sites, just like a bedspread which is tucked-in under a mattress. Granule cell axons on their way to the molecular layer of the DCoN presumably represent the main input to the ectopic cartwheel cells, which, with few exceptions (Fig. 9E), develop fewer dendrites than the normally positioned cartwheel cells. The ectopic cartwheel cells situated along the dorsal acoustic stria coincide in position with the lacy elongate cells described by Hackney et al. (1990) with the Golgi method, and we suggest that the two cell populations are identical.

As mentioned above, immunostained fibers and puncta are absent or extremely rare in both the AVCoN and PVCoN, but in examining the nuclear complex in serial sections we have found a small bundle of thin (1–2 μm) fibers, at the ventral-most tip of PVCoN. These fibers form varicosities and terminal boutons within a small portion of the globular cell area (Fig. 10), but could not be traced to any of the afferent pathways; instead they appeared continuous with the lateral and caudal portion of the DCoN (Fig. 10D), where they may derive from a small group of cartwheel neurons or pyramidal neurons. Alternatively, they may originate from the descending fiber tract of Lorente de Nó (Fig. 4A). Furthermore, dense fiber staining is present in areas containing the extracerebellar projections of Purkinje axons (Figs. 1, 11), which continue past the deep cerebellar nuclei to innervate nearby brainstem regions; most of these axons terminate in the vestibular nuclei, but a small proportion project to the parabrachial nuclei, the nucleus of the solitary tract, and the prepositus hypoglossal nucleus (not shown; see also DeCamilli et al. 1984). The extracerebellar Purkinje cell axons form distinct bundles medially beneath the DCoN, in the vicinity of the restiform body and in the brachium conjunctivum (Figs. 1, 9, 11). Caudally (Figs. 10, 11), another bundle of Purkinje cell axons, which derives from the floccular peduncle, courses medialward around the restiform body and enters the brainstem near the border between the DCoN and PVCoN. This bundle, which runs under the intermediate and dorsal acoustic striae (arrowheads in Fig. 10A) to reach the vestibular nuclei, provides but few, if any, collaterals to the cochlear nuclear complex. The DAS, where pyramidal cell axons are found, appears barely immunostained above background. Only when the DAB reaction is excessively prolonged for 30 mins or when the reaction product is enhanced by osmication, does the DAS become faintly immunostained (Fig. 10A).

Immunoelectron microscopy

The densely immunostained DCoN neurons observed by light microscopy possess the ultrastructural features (Figs. 12, 13) characteristic of cartwheel neurons, as determined by the Golgi-EM method in rat (Wouterlood and Mugnaini 1984). Near the surface of the ultrathin section, where penetration of the antisera is maximal, all cartwheel neurons are immunolabelled; the cartwheel cell nuclei are densely stained, contain small, rather uniformly dispersed heterochromatin granules and often display one or more invaginations of the nuclear envelope (Figs. 12A, 13A). Short cisterns of granular endoplasmic reticulum are scattered in the perikaryon, or arranged into small stacks. Some of the subsurface cisterns are associated with mitochondria (Figs. 12, 13A, B), an important marker for this cell type (Wouterlood and Mugnaini 1984; Berrebi and Mugnaini 1988b). Additionally, peculiar assemblies of mitochondria and flattened cisterns with a narrow lumen are also seen in the deep cytoplasm (Fig. 13A, C). Axosomatic synapses are exclusively of the symmetric category, formed with boutons containing pleomorphic synaptic vesicles. Some of these boutons are immunolabelled (Fig. 13D). The ratio between PEP-19-positive and PEP-19-negative boutons, which may depend on the degree of penetration of immunoreagents, varies from cell to cell. The cartwheel cell shown in Fig. 12A has 6 immunopositive and 3 immunonegative axosomatic boutons, while the cell in Fig. 13A has 4 immunopositive and 5 immunonegative boutons. At the surface of the immunoreacted slice we have seen fragmented cartwheel neurons (not shown), damaged by the Vibratome blade, that are contacted by up to 10 immunoreactive boutons and rare immunonegative boutons. Since immunopositive boutons are found only near the very surface of the embedded Vibratome slice, a meaningful statistical evaluation of the proportion of PEP-19-positive and -negative boutons was not possible. When located deeper in the tissue slice, cartwheel neurons remain densely immunolabelled in their cytoplasm, but their nucleus appears unlabelled and all of their axosomatic boutons are immunonegative (Fig. 12B). The cell bodies of densely immunostained neurons situated along the stria and in the lamina and

Fig. 9A–E. These micrographs illustrate ectopic cartwheel neurons. **A** A row of ectopic cartwheel neurons (*arrows*) is situated adjacent to the dorsal and intermediate acoustic striae (*das/ias*) in this coronal section of the DCoN. *lam*, Granule cell lamina; *PCa*, Purkinje cell axons; *rb* restiform body. ×70. **B** Ectopic cartwheel neurons (*arrows*) situated at the border of (*top*) and within (*center* and *bottom*) the granule cell lamina (*lam*). Portions of DCoN layers 1 and 2 are included in this parasagittal section. ×125. **C** Group of ectopic cartwheel neurons in the deep DCoN from a horizontal section. This micrograph reveals densely stained cell bodies (*arrows*) and their dendritic arbors, as well as a faintly stained cell (*arrowhead*), tentatively identified as an ectopic pyramidal cell. *das*, Dorsal acoustic stria. ×230. **D** Ectopic cartwheel neuron (*arrow*) situated in the superficial granular layer (*sgl*) of the PVCoN. *t* Tenia of the choroid plexus. ×125. **E** Ectopic cartwheel neuron (*arrow*) at the medial border of the VCoN in correspondence with the medial sheet of granule cells. *rb*, Restiform body. ×190

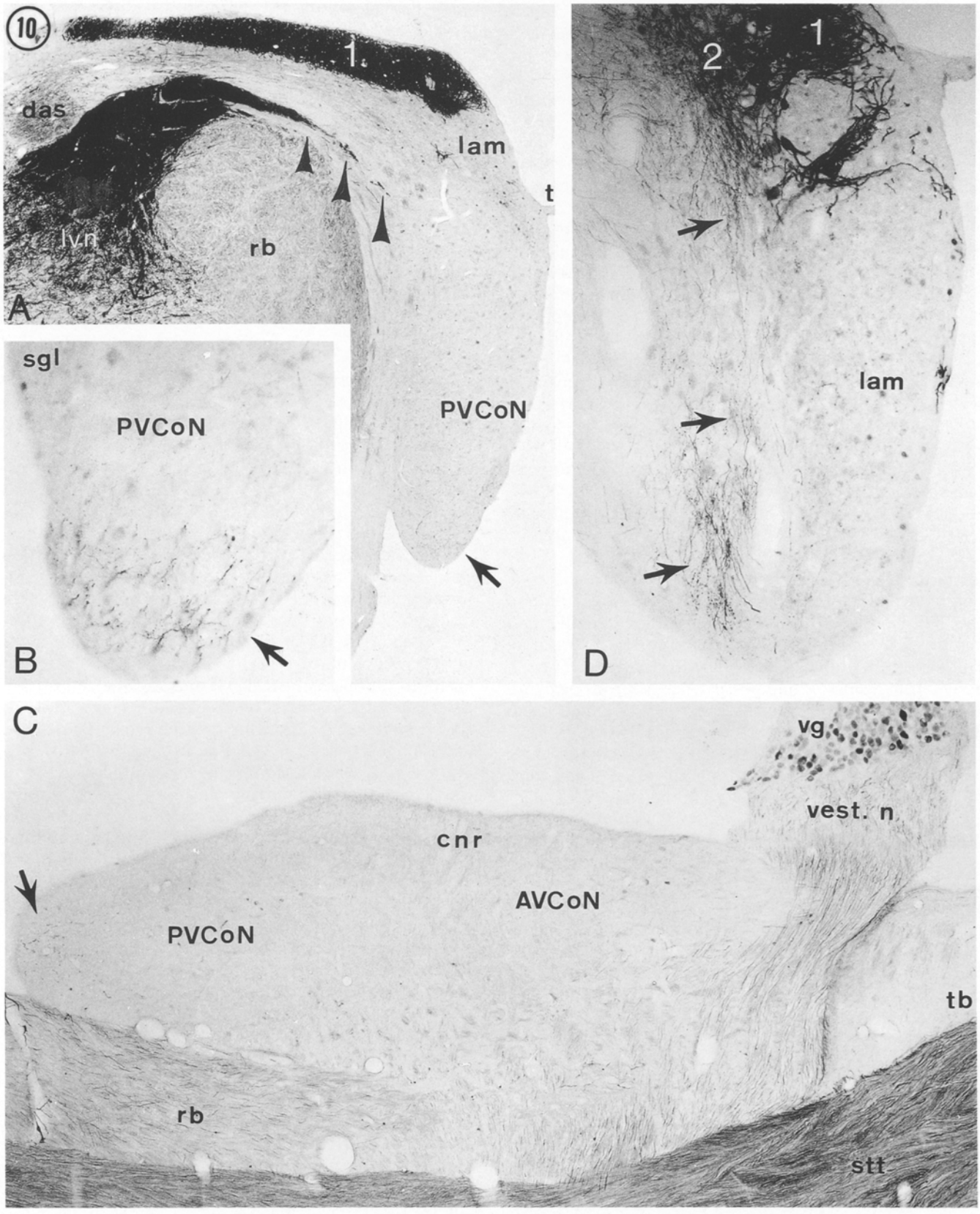
10
1
das
lam
t
lvn
rb
A
sgl
PVCoN
PVCoN
B
2
1
lam
D
C
vg
vest. n
cnr
AVCoN
PVCoN
tb
rb
stt

superficial granular layer, which are rarely encountered in thin sections, resemble those of cartwheel neurons in layers 1–2.

Densely immunoreactive cartwheel dendrites arise as thick main processes (Fig. 12B), branch near the cell soma and extend into the neuropil of layers 1 and 2. The dendritic branches possess a very high density of gemmular spines (Fig. 14). The spines contain a vesicular spine apparatus and usually form asymmetric synapses with immunonegative parallel fiber varicosities. Many of the immunostained axons in layers 1–3 resemble the cartwheel cell axons described in rat (Wouterlood and Mugnaini 1984). They are thinly myelinated and measure 0.6–2.5 μm in diameter, exclusive of their myelin sheaths (Fig. 15A, B). Many PEP-19-positive boutons containing pleomorphic vesicles contact the main-stem dendrites of cartwheel cells (Fig. 14), but relatively few are observed forming synapses with cartwheel cell dendritic spines (inset to Fig. 14) or the trunks of spiny branchlets. Some of the immunoreactive boutons are seen to arise from myelinated axons (Fig. 15A), but for the most part they originate from unmyelinated fiber branches of varying diameters (Fig. 15B, C). This suggests that cartwheel cell axons, in general, lose their myelin sheaths and give rise to thinner, unmyelinated fiber branches before forming terminal boutons.

While the cartwheel neurons usually appear distinctly immunolabelled, the cell bodies and dendrites of pyramidal neurons appear faintly immunostained in the electron microscope. This moderate immunoreactivity, like that of the cartwheel cell nuclei and boutons, is detectable only at the periphery of the slices. In many sections we noted that the immunoreaction product faded away within a distance of only 2–3 μm from the surface. The surface of the soma and emerging dendrites of both the apical and basal arbors are covered with boutons (Fig. 16A–C), many of which are immunoreactive, contain pleomorphic vesicles and form symmetric synapses. Some asymmetric synapses formed with boutons containing round vesicles are also seen on pyramidal cells, but these boutons are always immunonegative (Fig. 16C). Many PEP-19-positive boutons in layer 3 form synapses with small non-immunoreactive dendrites (less than 2 μm in diameter), which may belong to pyramidal, vertical, giant or other unidentified cells.

We have on occasion found immunoreactive boutons forming symmetric synapses with either a layer 1 stellate cell, a stellate cell dendrite (Fig. 17), a Golgi cell in layer 2 (not shown), or an unidentified medium sized neuron in layer 3 (not shown). We surmise that stellate and Golgi cells account for only a small proportion of cartwheel cell synaptic targets. Vertical cells in layer 3 were not identified in these experiments, nor did we study cells in layer 4 that were in contact with PEP-19-positive boutons (see Fig. 8F).

Discussion

The present study provides details of the intrinsic neuronal microcircuit within the superficial layers of DCoN that could only have been uncovered by revealing cartwheel neurons in their entirety. In a previous Golgi-EM investigation in the rat, the synaptic target of the cartwheel cell could not be determined, because its myelinated axon was not impregnated (Wouterlood and Mugnaini 1984). Therefore, we have examined the distribution and targets of the cartwheel axon using an antise-

Fig. 10A–D. These micrographs illustrate a bundle of PEP-19-positive fibers (*arrows*) that innervate the caudal rim of the PVCoN, beneath the superficial granular layer. **A** The PEP-19-positive bundle (*arrow*) in the PVCoN, which is hardly visible at this low magnification, appears unrelated to Purkinje cell axons. A bundle of Purkinje cell axons (*arrowheads*) can be followed from the border of the PVCoN to the vestibular nucleus. In serial sections, this bundle is seen to originate from the flocculus (*see open arrows in Fig. 11B*). The dorsal acoustic stria (*das*) contains little immunoreactivity, even in this osmium-tetroxide enhanced coronal section. The densely immunoreactive DCoN molecular layer (labelled *1*) and lateral vestibular nucleus (*lvn*) are also shown. *lam*, Granule cell lamina; *rb*, restiform body; *t*, tenia. ×40. **B** In this coronal section, the PEP-19-positive fiber bundle (*arrow*) at the caudal rim of PVCoN forms a number of axon terminals in correspondence with large neurons. *sgl*, Superficial granular layer. ×250. **C** The immunoreactive fibers and terminals in the caudal-most tip of PVCoN appear unrelated to the immunoreactive vestibular fibers in this ventral horizontal section. *cnr*, Cochlear nerve root; *rb*, restiform body; *stt*, spinal trigeminal tract; *tb*, trapezoid body; *vest. n.*, vestibular nerve; *vg*, vestibular ganglion. ×55. **D** In this coronal section, taken near the caudal-most and lateral portion of DCoN, it is apparent that the fiber bundle (*arrows*) shown in A–C courses beneath the lamina (*lam*) and can be followed from the lateral portion of layers 1–2 of DCoN. ×125

Fig. 11. A This medial parasagittal section demonstrates cerebellar Purkinje axons (*open arrows*) that course past the DCoN on their way to the vestibular nuclei. A small cluster of ectopic cartwheel neurons (*thick arrow*) can also be seen ventral to layer 3 of the DCoN. Layer 4 is not present at this medial level. *CN*, Cerebellar nuclei; *das/ias*, dorsal and intermediate acoustic striae; *rb*, restiform body; *svn*, spinal vestibular nucleus. ×80. **B** In horizontal section, it is clear that the bundle of Purkinje cell axons shown in **A** (*open arrows*) arises from the flocculus (*floc*) and curves around the restiform body (*rb*) to enter the corticocerebellar-vestibular fiber tract (*ccvf*). *Dashed line* marks the midline. *CV*, Cerebellar vermis; *bc*, brachium conjunctivum; *mcp*, middle cerebellar peduncle; *lam*, granule cell lamina. ×30

Fig. 12A, B. Electron micrographs of cartwheel neurons show their dense immunoreactivity. **A** This cell, located close to the periphery of an immunoreacted slice, possesses an immunolabelled nucleus (*N*), and is contacted by 6 immunopositive (*arrows*) and 3 immunonegative (*arrowheads*) axosomatic boutons. *Open arrow* points to a subsurface cistern-mitochondrion complex (*SC-M*), a characteristic feature of cartwheel neurons. *bc*, Blood capillary. ×6800. **B** This cell, situated deeper in the tissue slice, displays an immunonegative nucleus (*N*), and all of its axosomatic and axodendritic boutons (*arrowheads*) are PEP-19-negative. *Open arrow* marks a SC-M complex in the large dendritic stem. A portion of another immunolabelled cartwheel cell is present in the upper-left-hand corner. *bc*, Blood capillary. ×6800

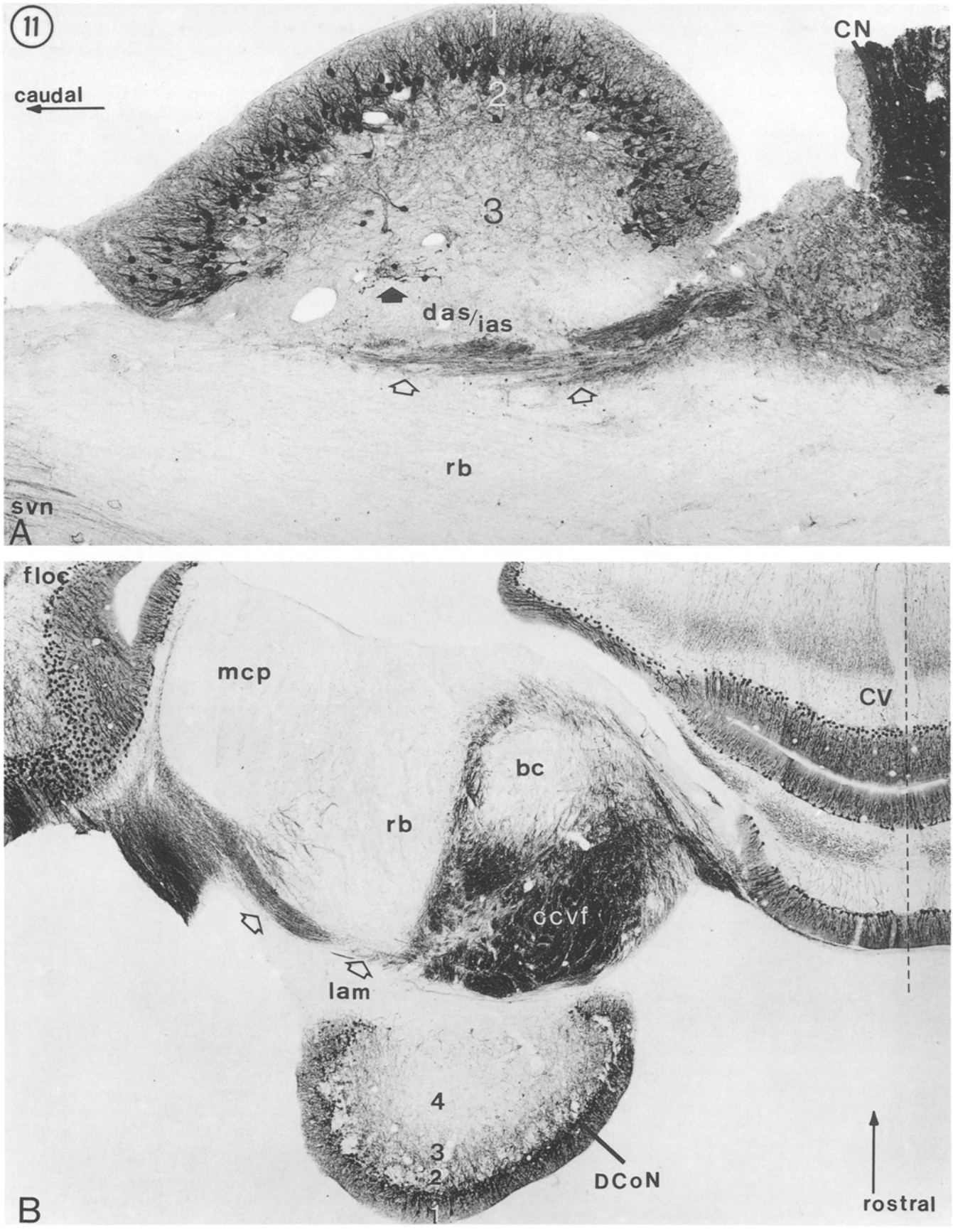
11
caudal
1
2
3
CN
das/ias
rb
svn
A
floc
mcp
CV
bc
rb
ccvf
lam
4
3
2
1
DCoN
rostral
B

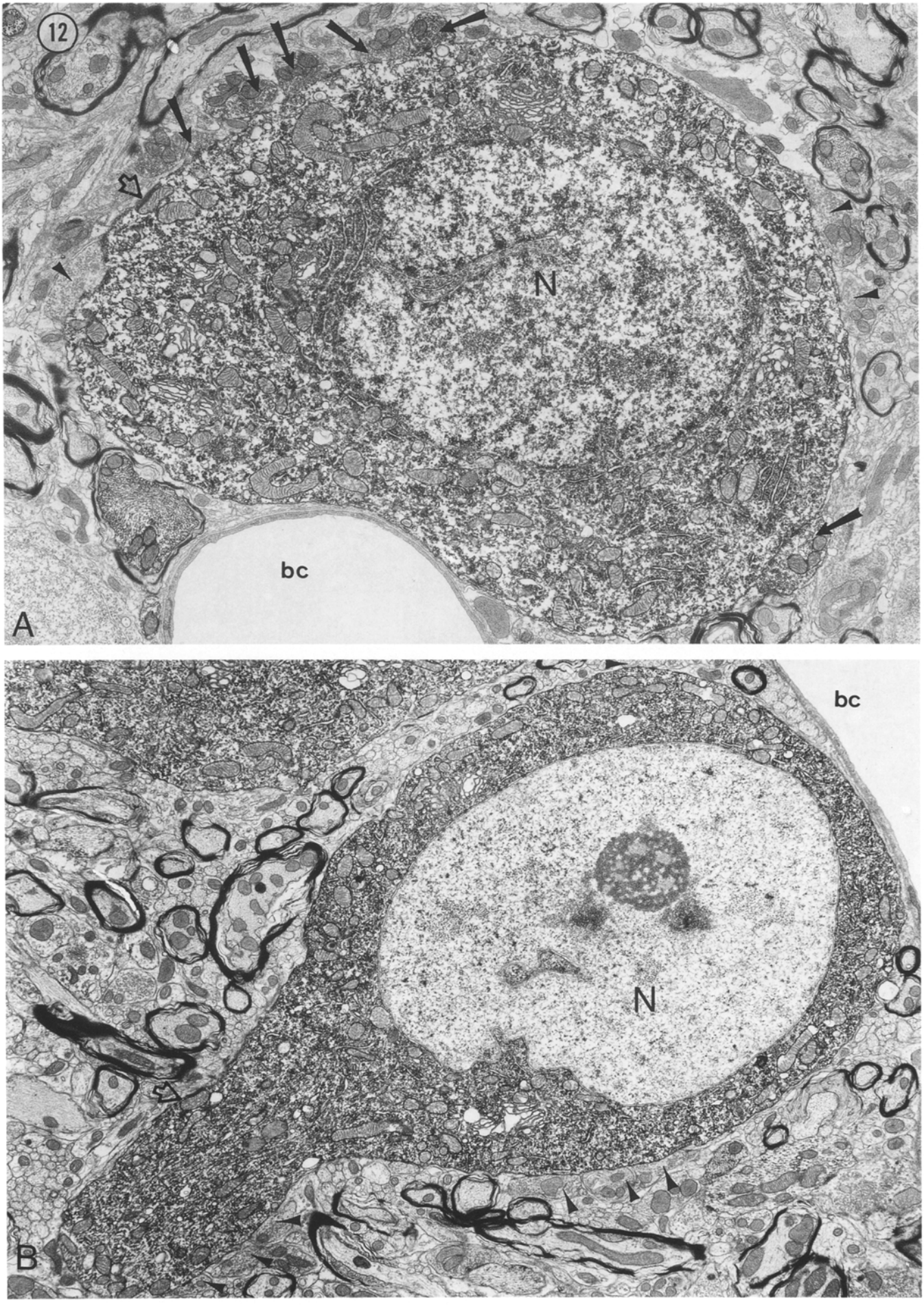
12
N
bc
A
bc
N
B

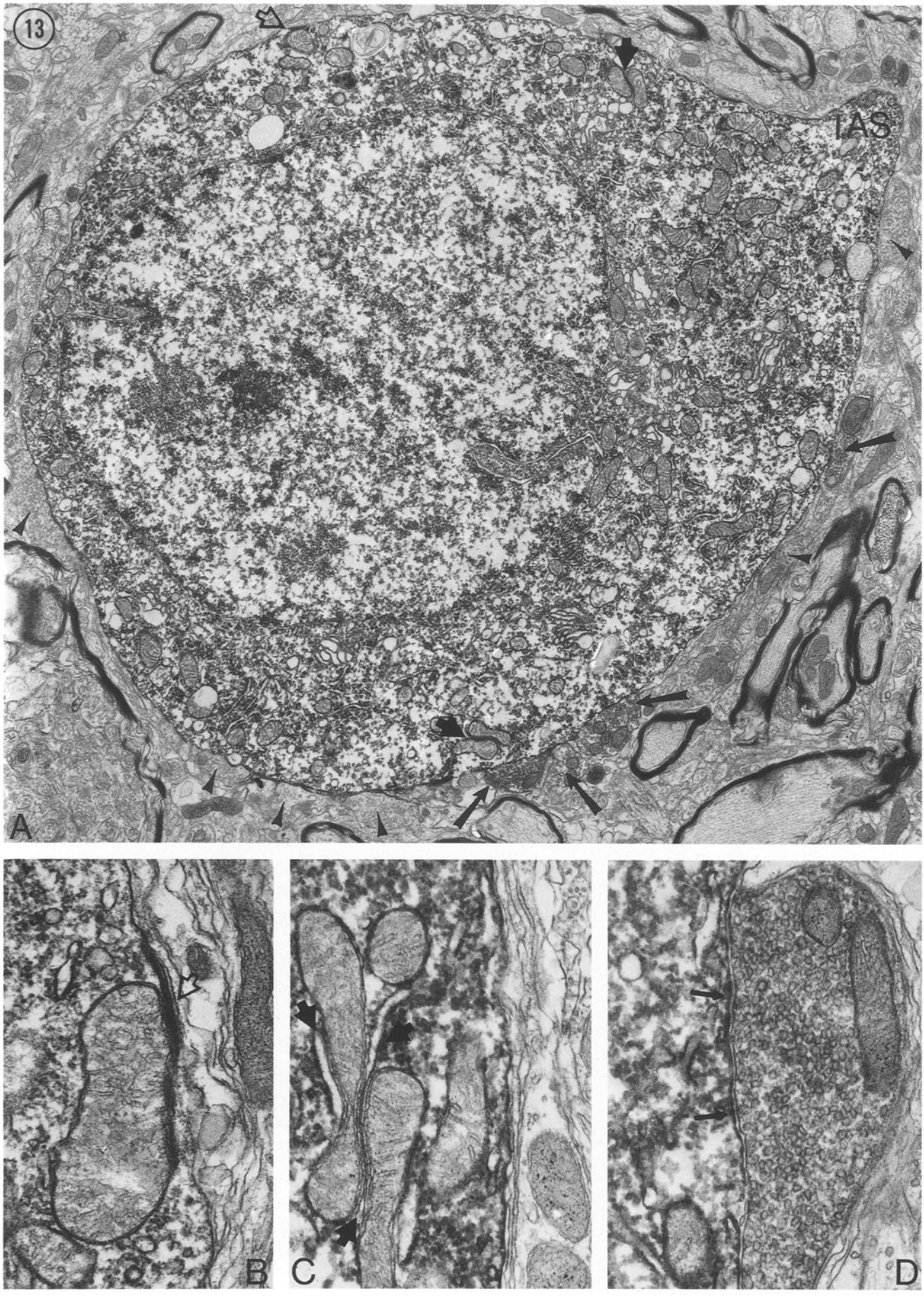
13
IAS
A
B
C
D

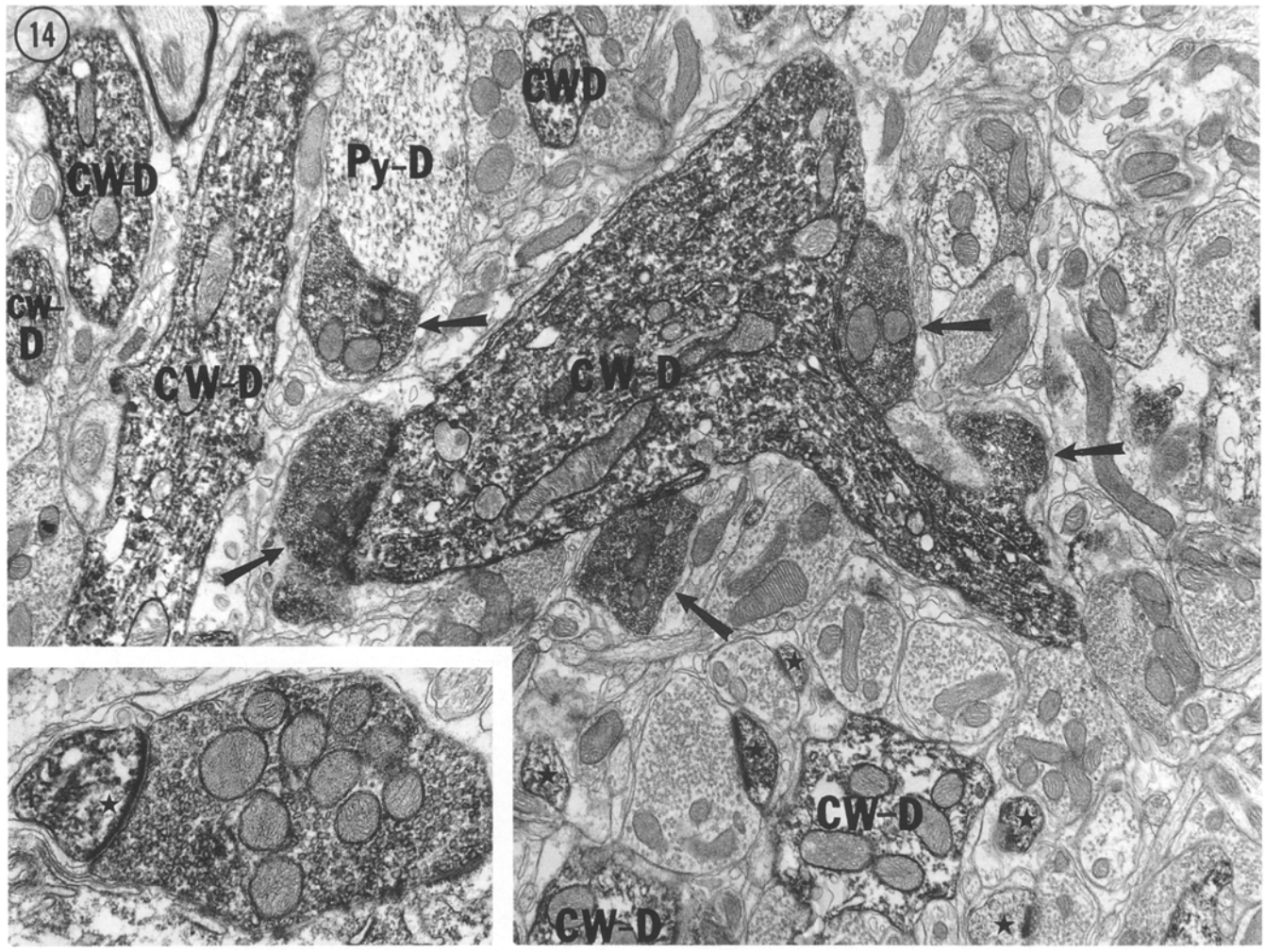

Fig. 14. This electron micrograph of the DCoN molecular layer shows 7 densely labelled cartwheel dendrites (*cw-D*) and 5 spines (*stars*). The principal cartwheel dendrite in the center of the field is contacted by 4 immunoreactive axon terminals (*arrows*). *Py-D*, Weakly immunoreactive pyramidal cell dendrite apposed to an immunoreactive axon terminal (*arrow*). ×12400. *Inset:* An immunopositive cartwheel axon terminal with pleomorphic vesicles forms a synaptic junction with an immunolabelled cartwheel dendritic spine (*star*). ×21600

rum raised against the polypeptide PEP-19 as an immunocytochemical marker. The guinea pig, with its relatively restricted PEP-19 distribution and distinctly laminated DCoN, served as an ideal subject for this study. Our data show that in the guinea pig hindbrain, neurons that are densely immunostained in both their cell bodies and processes are found primarily in the cerebellar cortex and cochlear nuclear complex. Within the cochlear nuclei, PEP-19 revealed the entire population of cartwheel neurons in DCoN, as well as those displaced in the VCoN. In the guinea pig DCoN, cartwheel cell bodies reside mainly at the transition between layers 1 and 2; their dendritic arbors pervade layer 1, where they interdigitate with the apical arbors of pyramidal cells, and their axons can often be followed to layers 2–3, where they form a PEP-19-positive axonal plexus with a predominant transstrial orientation. This planar distribution, which is schematically illustrated in Fig. 18, coincides with the reported transstrial distribution of the basal dendritic arbors of pyramidal cells in the feline DCoN (Blackstad et al. 1984). Although we cannot exclude the possibility that some other fibers contribute to this plexus, it is clear that it consists primarily of cartwheel cell axons. The strong immunoreactivity in cartwheel cell bodies continues into their axons, and by

Fig. 13. A This electron micrograph illustrates a cartwheel neuron from layer 2 of DCoN with dense immunoreaction product in its soma. The cell is in contact with 4 immunoreactive (*arrows*) and 5 immunonegative (*arrowheads*) axosomatic boutons. *Open arrow* marks a SC-M complex. Peculiar assemblies of cisterns and mitochondria (*thick arrows*) are also encountered in the perikaryon. *IAS*, Initial axon segment. ×9300. **B** SC-M complex (*open arrow*) within an immunoreactive cartwheel neuron is shown here at higher magnification. ×43000. **C** Cisterns of endoplasmic reticulum (*thick arrows*) are apposed to mitochondrial profiles, or sandwiched between mitochondria. ×43000. **D** Immunoreactive bouton with pleomorphic synaptic vesicles forms symmetric synapses (*small arrows*) with a cartwheel cell body. ×43000

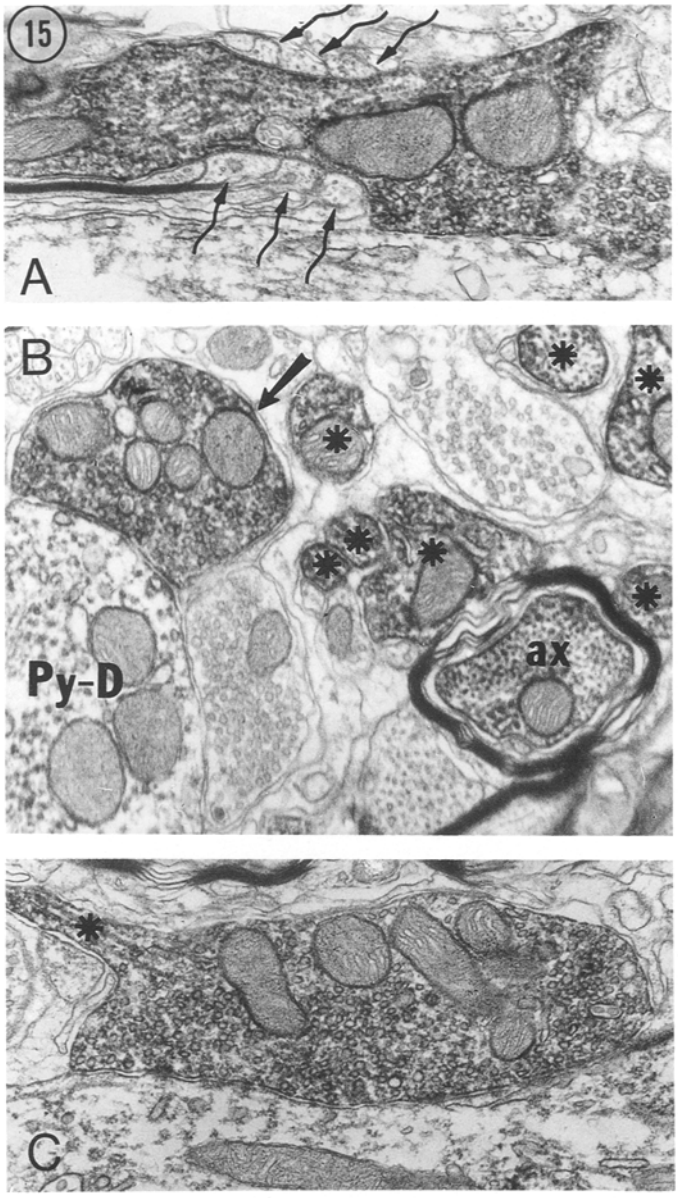

Fig. 15A–C. Electron micrographs from layer 3 showing PEP-19-positive fibers and boutons. **A** This micrograph illustrates a myelinated pre-terminal axon branch just prior to its formation of a terminal bouton. *Curved arrows* indicate oligodendrocytic paranodal loops at the termination of the myelin lamellae. ×29400. **B** A myelinated immunoreactive axon (*ax*) and numerous unmyelinated preterminal branches (*asterisks*) are evident in this micrograph. *Arrow* indicates immunoreactive axon terminal in contact with the weakly immunoreactive dendrite of a pyramidal cell (*Py-D*). ×29400. **C** An immunoreactive axo-dendritic terminal originates from an unmyelinated pre-terminal branch (*asterisk*). ×29400

analogy with the Purkinje cell, we assume that immunoreactivity extends all the way to the axon terminals (discussed further below). The PEP-19-positive boutons of cartwheel cell axons, like those of Purkinje cell axons, contain pleomorphic synaptic vesicles and make symmetric synaptic junctions. Presumably, they are inhibitory, in accordance with the GAD-like immunoreactivity of their parent cell bodies (Mugnaini 1985; Mugnaini and Oertel 1985; Moore and Moore 1987; Adams and Mugnaini 1987; Roberts and Ribak 1987).

Pyramidal cells, generally considered the sole projection neurons in the superficial layers of the DCoN, were shown to receive numerous symmetric synapses from PEP-19 immunostained terminal boutons on their apical dendritic shafts, cell bodies and basal arbors. Our data, therefore, strongly suggest that pyramidal cells represent a primary target of the cartwheel axon.

In a quantitative study of the cat DCoN, Smith and Rhode (1985) reported that 90% of the synaptic contacts formed on pyramidal cell bodies, and most of those on the axon hillock, are of the pleomorphic vesicle category. This same type of bouton accounted for a significant portion of the innervation on the proximal apical (33%) and basal (35%) dendrites. Our data in the guinea pig indicate that a proportion of these boutons belong to cartwheel cell axons. Cartwheel cells display both GABA-like and glycine-like immunoreactivities in various mammals (Wenthold et al. 1986, 1987; Osen et al. 1987, 1990). In the guinea pig, in which no stellate cells and only a small proportion of layer 3 cells display this dual labelling, at least a subpopulation of GABA- and glycine-like immunoreactive boutons on pyramidal cell bodies (Osen et al. 1990; see also Wenthold and Hunter 1990) may correspond to the PEP-19-positive cartwheel cell boutons demonstrated here.

Cartwheel neurons were also studded with immunopositive boutons on their cell bodies and primary dendrites, indicating an existing system of recurrent collaterals whose geometrical orientation remains to be established (Fig. 18). Since the layer 3 vertical cell (Lorente de Nó 1981) also possesses dendritic fields situated in the territory of the cartwheel axons (Osen et al. 1990), it may represent a possible third site of cartwheel cell innervation. A revised plan of the intrinsic microcircuit of the superficial layers of the DCoN is schematically illustrated in Fig. 19. This diagram complements previous schemes which did not include the identified cartwheel cell axon. Although the cell bodies of many giant cells lie outside of the layer 3 plexus, the dendrites of at least some types of giant cells are found in layer 3. Therefore, these cells should also be considered potential targets of cartwheel axons, although they have not been included in our scheme. Some of the cells in layer 4, that are provided with ascending dendrites outlined by PEP-19-positive boutons, could represent a class of giant cells. These may correspond to neurons described by Osen et al. (1990) as being covered, like the pyramidal cell bodies, with boutons labelled by GABA and glycine antisera. Moreover, the weakly immunoreactive deep cells may represent displaced pyramidal neurons.

We have also identified a small fiber bundle that appears to originate from the medial edge of the DCoN and run along the caudal rim of the PVCoN to innervate a region occupied predominantly by globular cells (Hackney et al. 1990). This projection, which may derive from a subpopulation of cartwheel or pyramidal cells, or belong to a small pool of descending fibers in the tract described by Lorente de Nó (1933), has not been

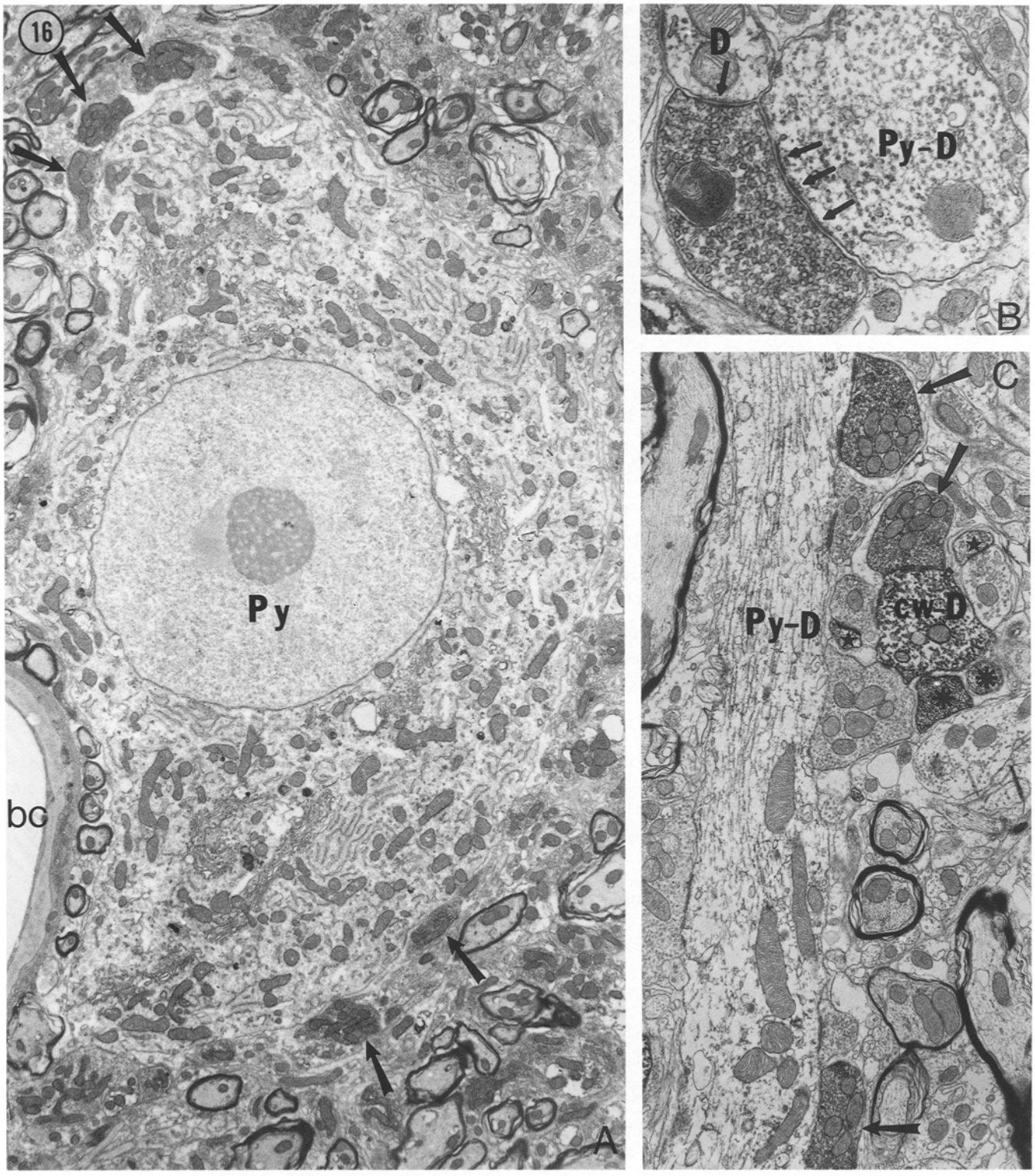

Fig. 16. A Five immunoreactive axosomatic boutons (*arrows*) contact a pyramidal cell body (*Py*) in layer 2 of DCoN. The pyramidal cell contains only a barely perceptible amount of reaction product. *bc*, Blood capillary. ×4900. **B** Detail of an immunoreactive bouton, containing pleomorphic vesicles, in synaptic contact with a weakly immunoreactive pyramidal cell dendrite (*Py-D*) and another small dendrite (*D*) in layer 3. *Small arrows* point to symmetric postsynaptic densities. ×29500. **C** This faintly positive apical dendrite of a pyramidal cell (*Py-D*) at the border of layers 1 and 2 is in synaptic contact with 6 terminal boutons. Two of these (*large arrows*) are densely immunoreactive and contain pleomorphic synaptic vesicles. Also shown is a cartwheel cell dendrite (*cw-D*) forming a symmetric synapse with an immunoreactive bouton (*large arrow*). Immunoreactive cartwheel dendritic spines (*stars*) and unmyelinated axons (*asterisks*) are also indicaed. ×9600

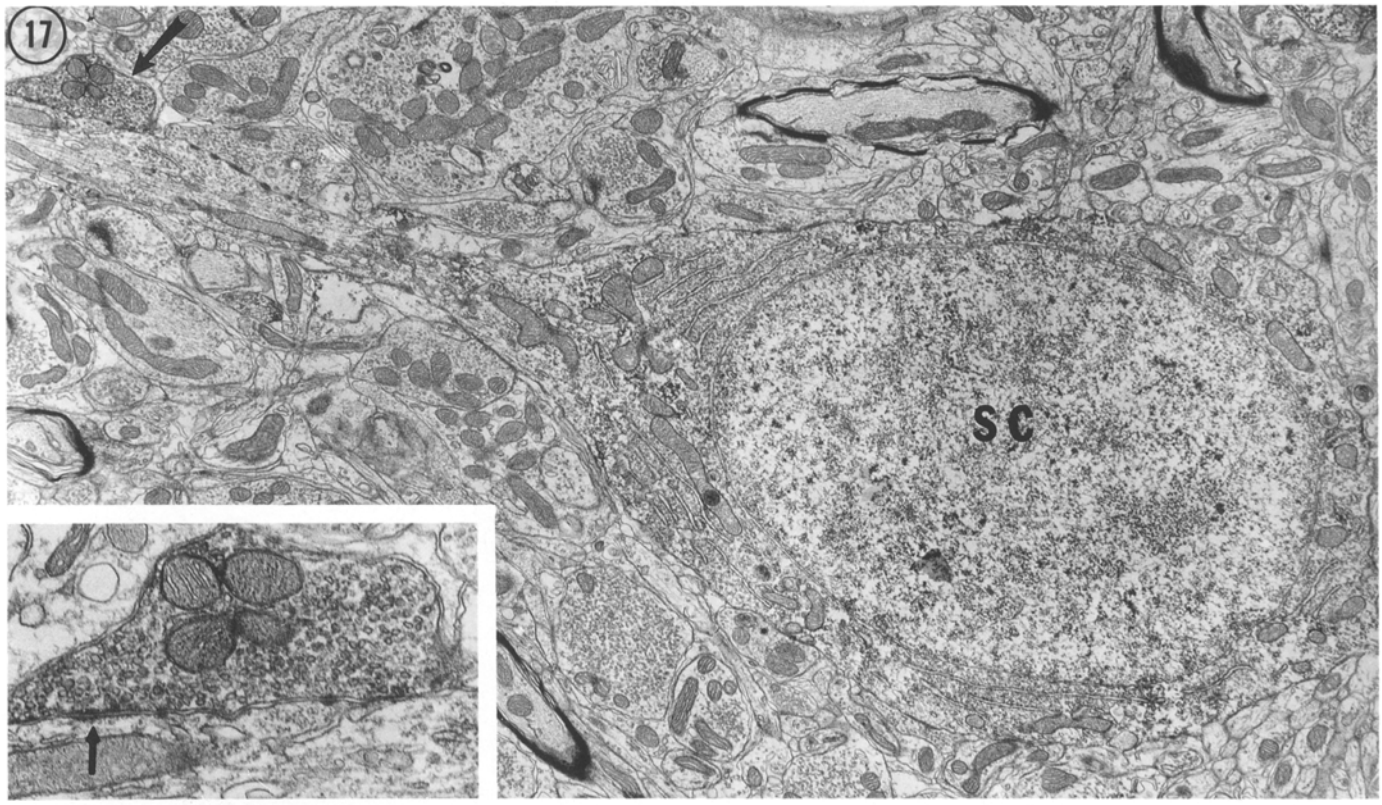

Fig. 17. This electron micrograph demonstrates a synapse between a cartwheel axon terminal (*arrow*) and the main stem dendrite of a layer 1 stellate cell (*SC*). ×8600. *Inset:* Higher magnification of this synapse shows that the bouton contains pleomorphic vesicles and forms a symmetric synaptic junction (*small arrow*). ×29400

previously recognized as a separate entity, and its precise origin needs to be ascertained with appropriate tract-tracing methods. Previously, a tonotopically organized pathway from the DCoN to the VCoN has been reported (Wickesberg and Oertel 1988), but the projection neurons, the vertical cells of the ventrotubercular tract, are confined to the deep DCoN region (Lorente de Nó 1933) and are PEP-19-negative.

Considerations of cellular and nuclear geometry

Previous studies have pointed out that the DCoN is organized anisotropically, with the parallel fibers running in the strial direction, the primary cochlear fibers in the transstrial direction, and the flattened arbors of pyramidal neurons and vertical cells also oriented transstrially. This dendritic anisotropy is particularly evident for the basal arbor of pyramidal neurons, which occupies layer 3, in register with the terminal arborizations of the primary fibers (Blackstad et al. 1984). Our data indicate that the cartwheel cell axons also synapse on the pyramidal cell basal arbors, and conform to the predominant transstrial orientation of cell processes in layer 3. While in cat the cartwheel cell dendrites form nearly spherical fields, in the guinea pig they may be anisotropic, as their stems appear to diverge more in the transstrial than in the strial direction, although their high density makes it difficult to ascertain this point unequivocally. In Fig. 20, where the principles of cellular geometry in the DCoN are schematically illustrated, we have represented the cartwheel dendritic field slightly longer transstrially. It should be pointed out that although we have demonstrated the predominant transstrial distribution of the cartwheel axonal plexus, we cannot assess the precise spatial distribution of individual cartwheel axons with respect to the DCoN isofrequency bands (Rose et al. 1959; Sando 1965; Ryan et al. 1988). It is probable that individual cartwheel axons are distributed immediately beneath their parent perikarya (as shown in Fig. 20A, cell I), but we cannot exclude that the axonal field is larger and that each cell may produce lateral inhibition within the same band (Fig. 20A, cells II–IV) or in immediately adjacent bands (Fig. 20A, cell V). Oertel and Wu (1989) have shown a HRP-labelled cartwheel cell which formed a dense axonal plexus in layer 2 of the mouse DCoN (see their Fig. 3), but the axonal filling was incomplete. Complete labelling of individual cartwheel neurons by intracellular tracer injections can lead to a resolution of this problem.

Limitations

A possible criticism of our data arises from our interpretation that PEP-19 immunostained axons and terminal

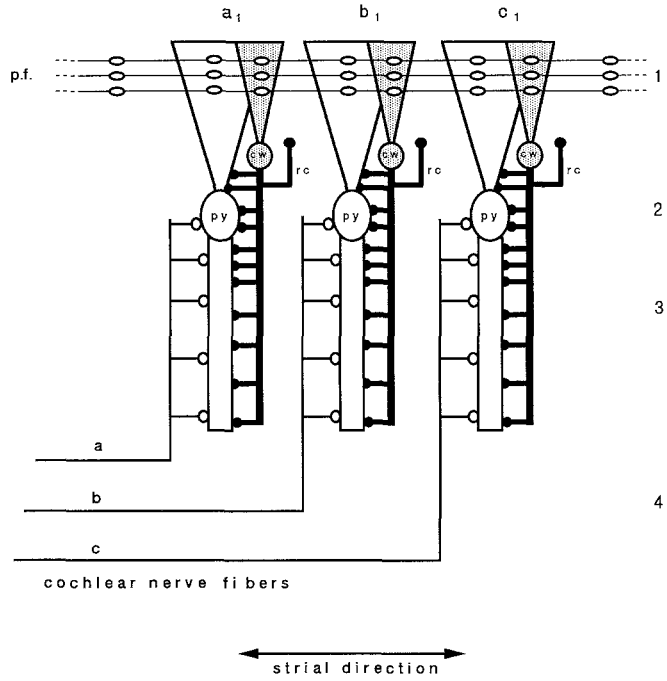

Fig. 18. This diagram shows three major sources of innervation of pyramidal cells (*py, white*) and the distribution of the axons (*solid black*) of cartwheel cells (*cw, stippled*) as viewed in the strial plane. The DCoN layers are indicated by Arabic numerals. Isofrequency bands are marked a_1, b_1 and c_1. Pyramidal cell basal dendritic arbors are flattened in this view, as are the cartwheel axonal plexuses, although their actual dimensions remain to be established. Cochlear nerve fibers (*a, b* and *c*) form tonotopically organized excitatory synapses (*open boutons*) on the cell bodies and basal arbors of pyramidal neurons. The excitatory parallel fibers (*p.f.*), which course across isofrequency bands, form varicosities (*open ellipses*) which contact the apical dendrites of pyramidal cells (*white*) and the cartwheel dendritic arbors (*stippled*). The inhibitory cartwheel axon terminals (*solid black boutons*) form numerous synapses upon the cell bodies and the basal and apical dendrites of pyramidal cells, here drawn within the same isofrequency bands. The geometrical orientation of recurrent collaterals (*rc*) of cartwheel axons, which form synapses with cartwheel and stellate cells, as well as the apical arbors of pyramidal neurons, remains to be assessed. Other cell types in layers 1–4 are not shown

boutons in DCoN must largely be intrinsic to the nucleus and represent cartwheel axons and terminals.

Our investigations on the distribution of this peptide in brain show that neurons which are intensely stained in their cell bodies and dendrites, such as Purkinje cells (Fig. 2), and thalamic, striatal and habenular projection neurons (Dino, Morgan and Mugnaini, unpublished observations), show dense immunoreactivity all along their fibers and terminal arborizations as well. We suppose, therefore, that the cartwheel cell population conforms to this rule (Fig. 21A) and that other moderately immunostained neurons in the auditory brainstem do not have densely stained axon terminals (Fig. 21B). Admittedly, however, neuronal types are very diversified, and one cannot exclude that categories of neurons within the cochlear nuclei, or in the acoustic brainstem nuclei which may provide inputs to the DCoN, are moderately or even weakly immunostained in their cell bodies and dendrites but accumulate peptide in the distal portions of their axons and in axon terminals (Fig. 21C). For example, the pyramidal cells are weakly immunoreactive, but they might form PEP-19-positive axon collaterals which remain in the DCoN or reach specific portions of the VCoN (see Fig. 10). Such collaterals have been shown in a small sample of intracellularly labelled pyramidal cells in cat (Smith and Rhode 1985), but have not been demonstrated in mouse (Oertel and Wu 1989) or guinea pig (Manis 1990). However, our sample of PEP-19-positive boutons within layers 1–3 of the DCoN contain pleomorphic synaptic vesicles and form symmetric synaptic junctions, whereas the axon collaterals of pyramidal cells in the cat contain round synaptic vesicles and form asymmetric contacts (Smith and Rhode 1985). In preembedding immunoelectron microscopy, sampling of axonal boutons is limited by the shallow penetration of immunoreagents in Vibratome slices of well-fixed brains, and small contingents of immunostained boutons provided with morphological features putatively different from those described in this paper may have escaped our scrutiny. Another shortcoming of the preembedding approach used in our studies is that we cannot determine what proportion of the presumed inhibitory boutons which synapse upon cartwheel and pyramidal neurons belong to cartwheel cell axons. This determination is important, because other kinds of neurons within the cochlear nuclei and acoustic brainstem may contribute to the inhibitory modulation of cells situated in the superficial layers of DCoN. Some inhibitory connections of stellate and vertical neurons in the DCoN (see review of Osen et al. 1990) are tentatively indicated by dashed lines in Fig. 19. This compelling question will require additional efforts with approaches yet to be developed.

Physiological/functional considerations

The intrinsic neuronal microcircuit of the DCoN superficial layers is involved in complex acoustic signal transformations (Young 1984), although its precise role in the processing of auditory information is not understood (Masterton and Granger 1988). The descending branches of the cochlear nerve fibers and the parallel fibers represent the two main excitatory pathways to the pyramidal cells. The cochlear input is tonotopically organized (Sando 1965; van Noort 1969; Noda and Pirsig 1974; Arnesen and Osen 1978) and largely restricted to their smooth, basal dendrites (Osen 1970; Cohen et al. 1972; Manis and Brownell 1983; Smith and Rhode 1985). Although the pyramidal cells receive direct eighth nerve innervation, their responses to sound reflect significant neuronal integration (Godfrey et al. 1975; Young and Brownell 1976; Rhode et al. 1983). Parallel fibers, the axons of cochlear granule cells, carry polysynaptic inputs and traverse isofrequency bands. Therefore, they do not respect tone specificity and are capable of spreading their effects across wide-frequency domains. Their synaptic contacts are made *en passant* with the spiny apical dendrites of the pyramidal cells (Kane 1974; Mugnaini et al. 1980a, b; Smith and Rhode 1985) and the

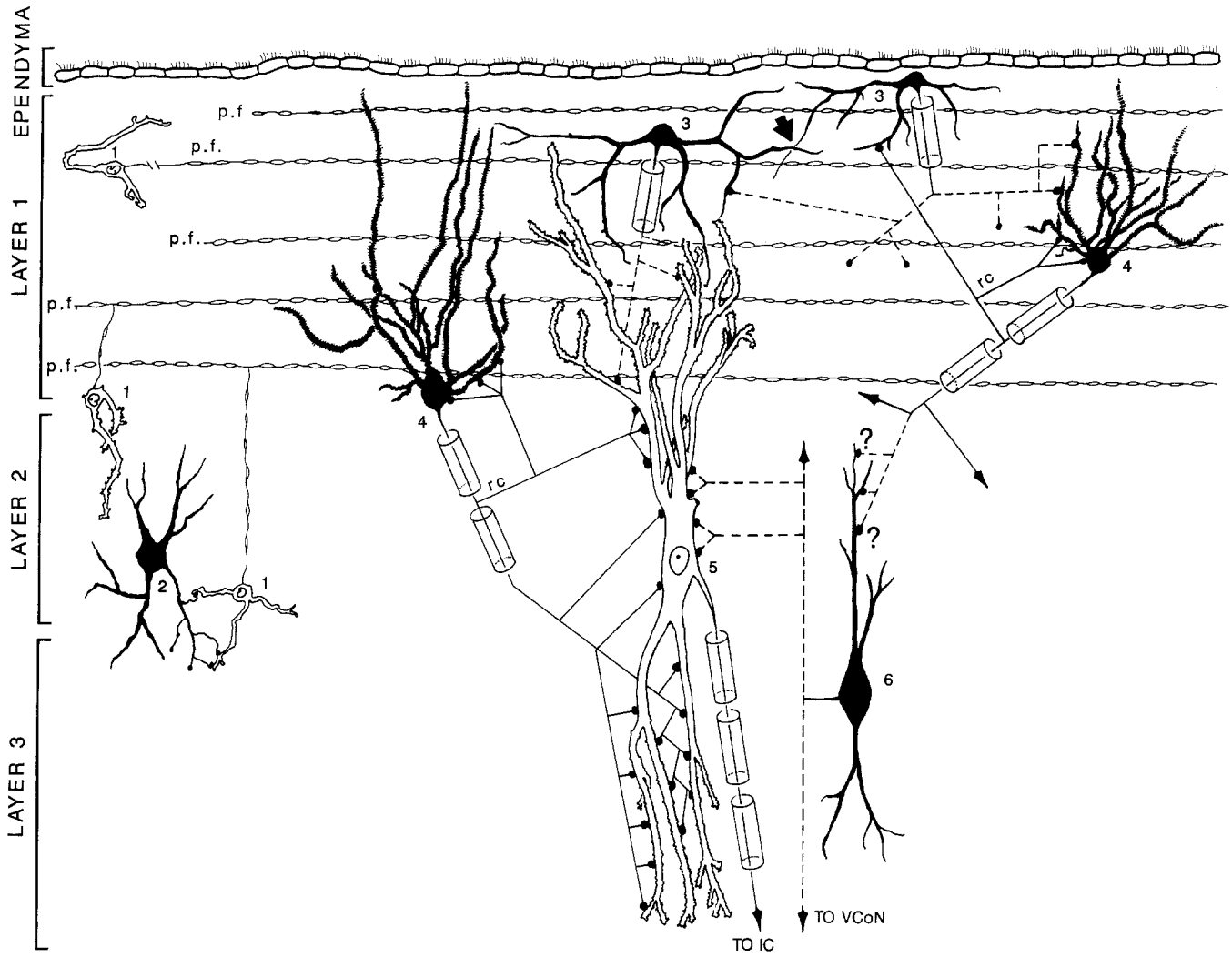

Fig. 19. Diagrammatic representation of the intrinsic neuronal circuitry in the superficial layers of DCoN. *Solid black cells* are presumed to be inhibitory (see review of Osen et al. 1990). Axons with proven connections are drawn with *solid lines*. *Dashed lines* indicate axons with connections yet to be directly demonstrated. Our data indicate that primary targets of cartwheel neurons (labelled *4*) are the cell bodies and apical and basal dendrites of the pyramidal neurons (labelled *5*). Cartwheel cell axons give rise to recurrent collaterals (*rc*) which synapse upon cartwheel cells and stellate cells (labelled *3*). The vertical neuron (labelled *6*) of *layer 3* may represent another, as yet unconfirmed, target. The *thick arrow* indicates a gap junction between stellate cell dendrites. Our unpublished observations show that such junctions between stellate cells are less frequently encountered in guinea pig than in rat (see Wouterlood and Mugnaini 1984). *1*, Granule cell; *2*, Golgi interneuron associated with granule cells; *p.f.*, parallel fibers

spine-laden dendrites of the cartwheel cells (Wouterlood and Mugnaini 1984; Oertel and Wu 1989). Parallel fiber synapses have been characterized as excitatory on anatomical (Mugnaini et al. 1980a, b; Oliver et al. 1983) and physiological grounds (Hirsch and Oertel 1988; Manis 1989), and exhibit pronounced paired-pulse potentiation and significant low-frequency tetanic potentiation (Manis 1989). Therefore, it has been proposed that the information transmitted by granule cells depends on their recent history of activity. While the granule cell/parallel fiber system appears to modulate the overall activity of pyramidal cells, the nature of the output of DCoN seems to be under the specific control of eighth nerve inputs, descending projections, and related DCoN interneurons. Physiological studies have confirmed that the superficial layers of DCoN must contain a population of intrinsic inhibitory neurons which are excited by the parallel fiber system (Hirsch and Oertel 1988; Manis 1988). Both cartwheel and stellate neurons may fit this role as they receive parallel fiber input (Wouterlood and Mugnaini 1984; Wouterlood et al. 1984) and contain putatively inhibitory neurotransmitters (Osen et al. 1990).

Our anatomical data indicate that the cartwheel neuron plays a key role in modulating pyramidal cell activity. Cartwheel cells are nearly three times as numerous as pyramidal cells (our preliminary data, based on cell counts in PEP-19 immunostained sections from the DCoN, indicate that approximately 2900 pyramidal cells and 7700 cartwheel cells can be found in the guinea pig DCoN). Furthermore, they form strategically located synapses on the cell bodies and proximal apical and

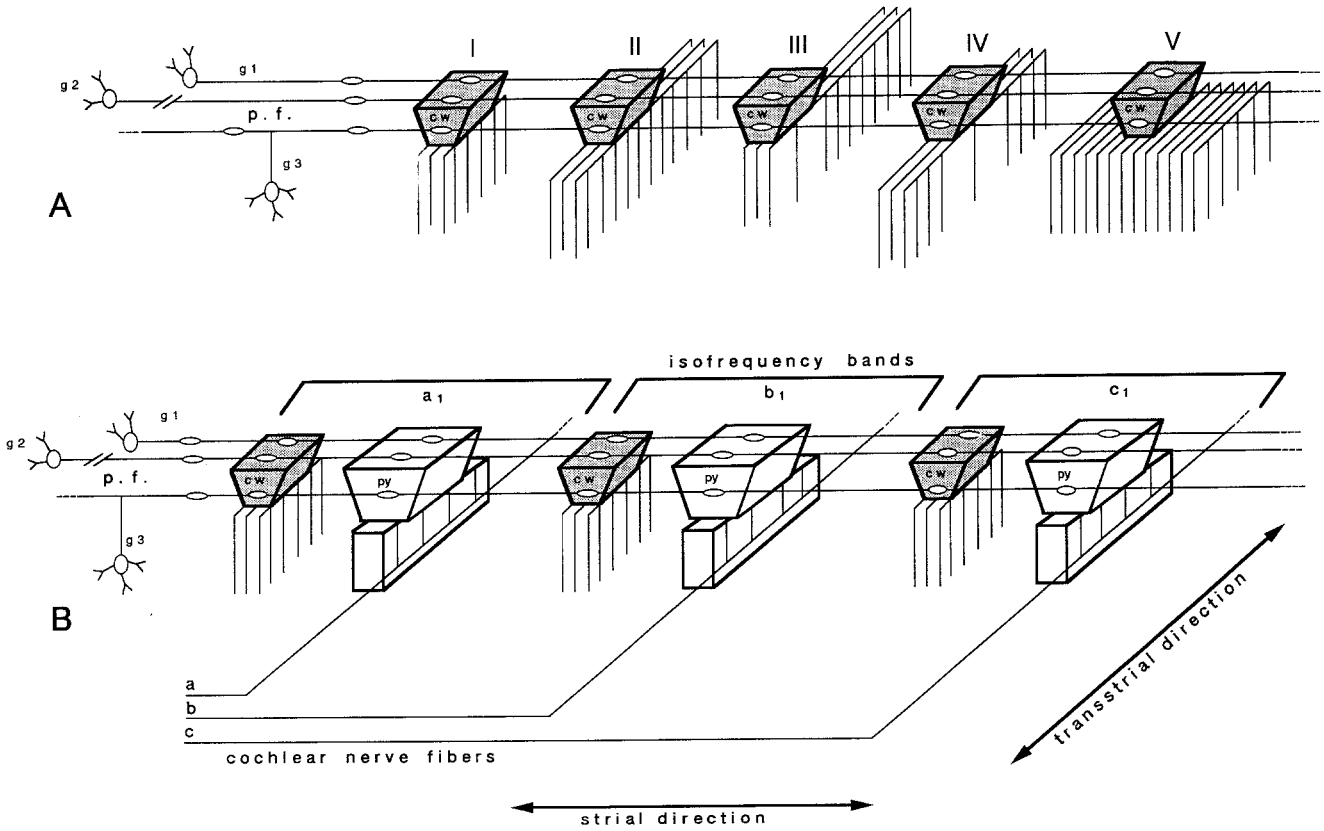

Fig. 20A, B. Schematic representation of cell geometry. **A** The predominant transstrial orientation of the axons (*solid lines*) of cartwheel neurons (*cw*) is compatible with different axonal arrangements, five of which have been illustrated in this scheme. Cartwheel cell dendrites (*stippled boxes*) form synapses with the varicosities (*open ellipses*) of parallel fibers (*p.f.*), the axons of granule cells (*g1–g3*). In cell *I*, the axon is distributed in a thin band approximately in register with the excitatory parallel fiber beam traversing the dendritic field, which is slightly elongated in the transstrial direction. In cell *II*, the arrangement is similar, but the axonal field extends farther away from the dendritic field. In cells *III* and *IV*, the axons form more connections off the parallel fiber beam than immediately beneath the dendritic field. In cell *V*, the numerous axonal branches have a predominant transstrial orientation, but occupy a wider territory in the strial direction, extending into neighboring isofrequency bands (see below). **B** The alignment of pyramidal cell dendritic arbors (*py*) along isofrequency bands (*a1–c1*) engendered by primary cochlear nerve fibers (*a–c*), according to Blackstad et al. (1984). In this diagram, we have inserted cartwheel neurons and their dendritic arbors (*cw, stippled*); their axonal arbors (*solid lines*) are depicted as flat sheets because of their preferred orientation in the transstrial direction (demonstrated in Fig. 7), using the simplest possible axonal arrangement represented in **A**. Actual dimensions of dendritic arbors and axonal plexuses remain to be determined. Cells are drawn separated from one another for the sake of clarity, although dendritic and axonal arbors of cells, in reality, overlap and interdigitate. *g1–g3*, Granule cells; *p.f.*, parallel fibers

basal dendrites of their targets. This type of synaptic arrangement may have important functional consequences. The putative inhibitory inputs (Mugnaini 1985; Wenthold et al. 1986, 1987; Osen et al. 1987, 1990) onto the soma and basal dendrites are in an optimal location for inhibition of synaptic currents (Rall 1964; Jack et al. 1975) from auditory nerve fiber synapses. This should make the pyramidal cells less responsive to sound. Cartwheel neurons are not contacted by primary fibers (Wouterlood and Mugnaini 1984), and their synapses on the proximal apical dendrites of the pyramidal neuron are well located to reduce the effectiveness of the parallel fiber synaptic input. In addition, hyperpolarization of the pyramidal cells may alter their subsequent discharge patterns (Manis 1990). Thus, cartwheel neurons are capable of profound modulation of the pyramidal cell response to both parallel fibers and cochlear nerve fibers.

Cartwheel cell axons also synapse with other cartwheel cells and with stellate cells, another category of putative inhibitory neurons (Mugnaini 1985; Osen et al. 1990) which receive parallel fiber input (Wouterlood et al. 1984). Stellate cell axons branch profusely in layers 1 and 2 (Lorente de Nó 1981) and may have as their main targets the dendrites and cell bodies of pyramidal, cartwheel and other stellate neurons (Fig. 19). Thus, in addition to inhibiting the pyramidal neurons, cartwheel cells may be involved in disinhibitory phenomena. Such complex interactions cannot be fully understood without precise knowledge about the geometrical and biophysical properties of both cartwheel and stellate neurons.

It should be noted that while classically considered an auditory relay nucleus, the DCoN has recently been proposed to perform integrative functions as well. Our laboratory has previously reported a heterogeneity in

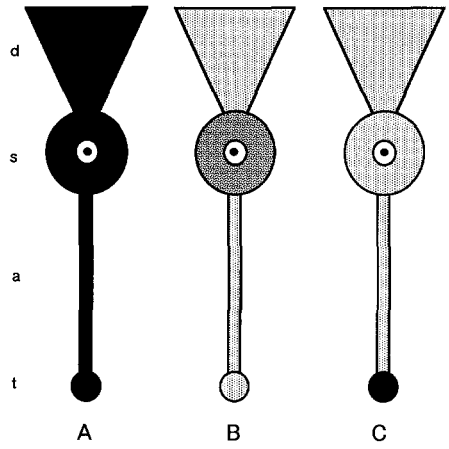

Fig. 21. The distribution of antigens within neurons can vary considerably, even between compartments of the same neuron. In case *A*, the antigen is strongly expressed throughout the entire neuron (*black*). Case *B* is an example of an antigen which is concentrated in cell bodies (*dense stipple*), but only weakly expressed in dendrites and axons (*light stipple*). Case *C* shows another antigen which is especially concentrated in axon terminals (*black*), but is scarcely present in cell bodies, axons and dendrites (*light stipple*). Case *C* is more representative of molecules involved in neurotransmission than of peptides such as PEP-19. *d*, Dendritic arborization; *s*, soma; *a*, axon; *t*, axon terminal

the morphology of mossy fiber terminals in the cochlear granule cell domain (Dunn et al. 1988, 1992), and we assume that these projections originate in various nuclei. Tract-tracing studies have demonstrated a pathway between the dorsal column nuclei, which relay somatosensory information, and the DCoN (Itoh et al. 1987; Weinberg and Rustioni 1987, 1989), suggesting a polysensory integrative role for the DCoN. Furthermore, by virtue of the fact that 2-deoxy-D-[^{14}C] glucose is utilized asymmetrically in the rabbit DCoN following Pavlovian conditioning (Harvey et al. 1988), it has been proposed that this nucleus may also play a role in associative learning involving auditory input.

Homology between DCoN cartwheel neurons and cerebellar Purkinje cells

Previously, we have proposed a homology between the DCoN cartwheel neuron and the cerebellar Purkinje cell. Both cell families synthesize GABA (Mugnaini 1985; Wenthold et al. 1986) and the peptide cerebellin (Mugnaini and Morgan 1987) and express other cell population markers such as PEP-19 (Mugnaini et al. 1987), calbindin (Berrebi et al. 1990), and the receptor for the inositol 1,4,5-trisphosphate intracellular second messenger (Mignery et al. 1989). Morphological differences between cartwheel and Purkinje cells have been highlighted elsewhere (Berrebi et al. 1990), and the demonstration that cartwheel neurons, but not Purkinje neurons, contain glycine-like immunoreactivity in addition to GABA-like immunoreactivity (Wenthold et al. 1986, 1987; Osen et al. 1990) stresses the fact that gene expression in the two cell populations is not identical. These considerations, however, do not exclude the notion of a cell lineage relationship.

Further support for the cartwheel cell/Purkinje cell homology is the finding that both cell types undergo degeneration in the murine mutations Purkinje Cell Degeneration, Lurcher and Staggerer (Berrebi et al. 1987, 1990) and express a similar mitochondrial anomaly in Nervous mutant mice (Berrebi and Mugnaini 1987, 1988b). Our experiments demonstrate similar functional roles for these two types of neurons within their respective environments: both serve to modulate the activity of the projection neurons which they innervate. However, the main targets of the Purkinje axon, neurons of the deep cerebellar nuclei, are found outside the cerebellar cortex while cartwheel neurons contact their targets, the pyramidal cells, within the DCoN superficial layers. It is interesting to note that target neurons of Purkinje cell axons are located within the cerebellar cortex in fish (Nieuwenhuys and Nicholson 1969). Furthermore, DCoN pyramidal cells display physiological properties which are similar, albeit not identical, to those of cerebellar nuclear neurons in guinea pig (Jahnsen 1986a, b; Llinás and Mühlethaler 1988a, b; Manis 1990).

Acknowledgements. We thank Dr. James I. Morgan for the generous gift of PEP-19 antiserum, and Drs. Joe C. Adams, Paul B. Manis, and Kirsten K. Osen for their invaluable criticism of an earlier form of the manuscript. This work was supported by PHS grant NS-09904.

References

Adams JC, Mugnaini E (1987) Patterns of glutamate decarboxylase immunostaining in the feline cochlear nuclear complex studied with silver enhancement and electron microscopy. J Comp Neurol 262:375–401

Arnesen AR, Osen KK (1978) The cochlear nerve in the cat: topography, cochleotopy and fiber spectrum. J Comp Neurol 178:661–678

Berrebi AS, Mugnaini E (1987) The dorsal cochlear nucleus in mutant mice. Anat Rec 218:17A

Berrebi AS, Mugnaini E (1988a) Targets and distribution of the cartwheel cell axon in the guinea pig dorsal cochlear nucleus. Soc Neurosci Abstr 14:489

Berrebi AS, Mugnaini E (1988b) Effects of the murine mutation 'nervous' on neurons in cerebellum and dorsal cochlear nucleus. J Neurocytol 17:465–484

Berrebi AS, Morgan JI, Mugnaini E (1987) Loss of cartwheel neurons in the dorsal cochlear nucleus of the mouse mutants, Lurcher, Purkinje Cell Degeneration and Staggerer. Soc Neurosci Abstr 13:1259

Berrebi AS, Morgan JI, Mugnaini E (1990) The Purkinje cell class may extend beyond the cerebellum. J Neurocytol 19:643–654

Blackstad TW, Osen KK, Mugnaini E (1984) Pyramidal neurons of the dorsal cochlear nucleus: a Golgi and computer reconstruction study in cat. Neurosci 13:827–854

Caspary DM (1990) Electrophysiological studies of glycinergic mechanisms in auditory brainstem structures. In: Ottersen OP, Storm-Mathisen J (eds) Glycine neurotransmission. Wiley, Chichester, pp 453–483

Caspary DM, Pazara KE, Kossl M, Faingold CL (1987) Strychnine alters the fusiform cell output from the dorsal cochlear nucleus. Brain Res 417:273–282

Cohen ES, Brawer JR, Morest DK (1972) Projections of the cochlea to the dorsal cochlear nucleus in the cat. Exp Neurol 35:470–479

DeCamilli P, Miller PE, Levitt P, Walter U, Greengard P (1984) Anatomy of cerebellar Purkinje cells in the rat determined by a specific immunohistochemical marker. Neurosci 11:761–817

Dunn ME, Vetter DE, Berrebi AS, Krider HM, Mugnaini E (1988) Different types of mossy fiber terminals in the guinea pig cochlear nucleus. Soc Neurosci Abstr 14:487

Dunn ME, Vetter DE, Berrebi AS, Krider HM, Mugnaini E (1992) The mossy fiber-granule cell-cartwheel cell system in the mammalian cochlear complex. In: Ainsworth WA, Evans EF, Hackney CM (eds) Advance in Speech, Hearing and Language Processing, Vol. III, Cochlear nucleus: structure and function in relation to modelling. JAI Press Ltd., London, in press

Friedrich VL Jr, Mugnaini E (1981) Electron microscopy: preparation of neural tissues for electron microscopy. In: Heimer L, Robards MJ (eds) Neuroanatomical tract-tracing methods. Plenum Press, New York, pp 345–376

Godfrey DA, Kiang NYS, Norris BE (1975) Single unit activity in the dorsal cochlear nucleus of the cat. J Comp Neurol 162:269–284

Hackney CM, Osen KK, Kolston J (1990) Anatomy of the cochlear nuclear complex of guinea pig. Anat Embryol 182:123–149

Harvey JA, Winsky L, Schindler CW, McMaster SE, Welsh JP (1988) Asymmetric uptake of 2-deoxy-D-[^{14}C] glucose in the dorsal cochlear nucleus during Pavlovian conditioning in the rabbit. Brain Res 449:213–224

Hirsch JA, Oertel D (1988) Synaptic connections in the dorsal cochlear nucleus of mice, in vitro. J Physiol (Lond) 396:549–562

Itoh K, Kamiya H, Mitani A, Yasui Y, Takada M, Mizuno N (1987) Direct projections from the dorsal column nuclei and the spinal trigeminal nuclei to the cochlear nuclei in cat. Brain Res 400:145–150

Jack JJB, Noble D, Tsien RW (1975) Electric current flow in excitable cells. Clarendon Press, Oxford University Press, London

Jahnsen H (1986a) Electrophysiological characteristics of neurones in the guinea-pig deep cerebellar nuclei in vitro. J Physiol (Lond) 372:129–147

Jahnsen H (1986b) Extracellular activation and membrane conductances of neurones in the guinea-pig deep cerebellar nuclei in vitro. J Physiol (Lond) 372:149–168

Kane ES (1974) Synaptic organization in the dorsal cochlear nucleus of the cat: a light and electron microscopic study. J Comp Neurol 155:301–330

Llinás R, Mühlethaler M (1988a) An electrophysiological study of the in vitro, perfused brain stem-cerebellum of the adult guinea-pig. J Physiol (Lond) 404:215–240

Llinás R, Mühlethaler M (1988b) Electrophysiology of guinea-pig cerebellar nuclear cells in the in vitro brain stem-cerebellum preparation. J Physiol (Lond) 404:241–258

Lorente de Nó R (1933) Anatomy of the eighth nerve. III. General plan of structure of the primary cochlear nuclei. Laryngoscope 43:327–350

Lorente de Nó R (1981) The primary acoustic nuclei. Raven Press, New York

Manis PB (1988) Intracellular recordings from pyramidal cells of the guinea pig dorsal cochlear nucleus. J Neurosci Meth 24:201

Manis PB (1989) Responses to parallel fiber stimulation in the guinea pig dorsal cochlear nucleus in vitro. J Neurophysiol 61:149–161

Manis PB (1990) Membrane properties and discharge characteristics of guinea pig dorsal cochlear nucleus neurons studied in vitro. J Neurosci 10:2338–2351

Manis PB, Brownell WE (1983) Synaptic organization of eighth nerve afferents to the cat dorsal cochlear nucleus. J Neurophysiol 50:1156–1181

Masterton RB, Granger EM (1988) Role of the acoustic striae in hearing: contribution of dorsal and intermediate striae to detection of noises and tones. J Neurophysiol 60:1841–1860

Mignery GA, Südhof TC, Takei K, DeCamilli P (1989) Putative receptor for inositol 1,4,5-trisphosphate similar to ryanodine receptor. Nature 342:192–195

Moore JK, Moore RY (1987) Glutamic acid decarboxylase-like immunoreactivity in brainstem auditory nuclei of the rat. J Comp Neurol 260:157–174

Mugnaini E (1985) GABA neurons in the superficial layers of the rat dorsal cochlear nucleus: light and electron microscopic immunocytochemistry. J Comp Neurol 235:61–81

Mugnaini E, Dahl A-L (1983) Zinc-aldehyde fixation for light microscopic immunocytochemistry of nervous tissues. J Histochem Cytochem 31:1435–1438

Mugnaini E, Morgan JI (1987) The neuropeptide cerebellin is a marker for two similar neuronal circuits in rat brain. Proc Natl Acad Sci USA 84:8692–8696

Mugnaini E, Oertel WH (1985) An atlas of the distribution of GABA-ergic neurons and terminals in the rat CNS as revealed by GAD immunohistochemistry. In: Björklund A, Hökfelt T (eds) Handbook of chemical neuroanatomy, vol 4. Elsevier, Amsterdam New York, pp 436–608

Mugnaini E, Osen KK, Dahl A-L, Friedrich VL Jr, Korte G (1980a) Fine structure of granule cells and related interneurons (termed Golgi cells) in the cochlear nuclear complex of the cat, rat and mouse. J Neurocytol 9:537–570

Mugnaini E, Warr WB, Osen KK (1980b) Distribution and light microscopic features of granule cells in the cochlear nuclei of the cat, rat and mouse. J Comp Neurol 191:581–606

Mugnaini E, Berrebi AS, Dahl A-L, Morgan JI (1987) The polypeptide PEP-19 is a marker for Purkinje neurons in cerebellar cortex and cartwheel neurons in dorsal cochlear nucleus. Arch Ital Biol 126:41–67

Mugnaini E, Dahl A-L, Morgan JI (1988) Cerebellin is a postsynaptic neuropeptide. Synapse 2:125–138

Nieuwenhuys R, Nicholson C (1969) Aspects of the histology of the cerebellum of mormyrid fishes. In: Llinás R (ed) Neurobiology of cerebellar evolution and development. American Medical Association, Chicago, pp 135–169

Noda Y, Pirsig W (1974) Anatomical projection of the cochlea to the cochlear nuclei of the guinea pig. Arch Otorhinolaryngol 208:107–120

Noort J van (1969) The structure and connections of the inferior colliculus. An investigation of the lower auditory system. Van Gorcum, Leiden

Oertel D, Wu SH (1989) Morphology and physiology of cells in slice preparations of the dorsal cochlear nucleus of mice. J Comp Neurol 283:228–247

Oliver DL, Potashner SJ, Jones DR, Morest DK (1983) Selective labeling of spiral ganglion and granule cells with D-aspartate in the auditory system of cat and guinea pig. J Neurosci 3:455–472

Osen KK (1970) Course and termination of the primary afferents in the cochlear nuclei of the cat. An experimental anatomical study. Arch Ital Biol 108:21–51

Osen KK (1985) "Ectopic" neurons of the cochlear nuclei. Neurosci Lett 22 [Suppl]:S167

Osen KK (1988) Anatomy of the mammalian cochlear nuclei: a review. In: Syka J, Masterton RB (eds) Auditory pathway-structure and function. Plenum Press, London New York, pp 65–76

Osen KK, Ottersen OP, Storm-Mathisen J (1987) Glycine-like immunoreactivity in the rat dorsal cochlear nucleus (DCN). Neuroscience 22 [Suppl]:S788

Osen KK, Ottersen OP, Storm-Mathisen J (1990) Colocalization of glycine-like and GABA-like immunoreactivities. A semi-quantitative study of individual neurons in the dorsal cochlear nucleus of cat. In: Ottersen OP, Storm-Mathisen J (eds) Glycine neurotransmission. Wiley, Chichester, pp 417–451

Rall W (1964) Theoretical significance of dendritic trees for neuro-

nal input-output relations. In: Reiss RF (ed) Neural theory and modeling. Proceedings of the 1962 Ojai Symposium. Stanford University Press, Standford, pp 73–97

Rhode WS, Smith PH, Oertel D (1983) Physiological response properties of cells labeled intracellularly with horseradish peroxidase in cat dorsal cochlear nucleus. J Comp Neurol 213:426–447

Roberts RC, Ribak CE (1987) GABAergic neurons and axon terminals in the brainstem auditory nuclei of the gerbil. J Comp Neurol 258:267–280

Rose JE, Galambos R, Hughes JR (1959) Microelectrode studies of the cochlear nuclei of the cat. Bull Johns Hopkins Hosp 104:211–251

Ryan AF, Furlow Z, Woolf NK, Keithley EM (1988) The spatial representation of frequency in the rat dorsal cochlear nucleus and inferior colliculus. Hear Res 36:181–190

Sando I (1965) The anatomical interrelationships of the cochlear nerve fibers. Acta Otolaryngol (Stockh) 59:417–436

Smith PH, Rhode WS (1985) Electron microscopic features of physiologically characterized, HRP-labeled fusiform cells in the cat dorsal cochlear nucleus. J Comp Neurol 237:127–143

Sternberger LA (1979) Immunocytochemistry, 2nd edn. Wiley, New York

Weinberg RJ, Rustioni A (1987) A cuneocochlear pathway in the rat. Neuroscience 20:209–219

Weinberg RJ, Rustioni A (1989) Brainstem projections to the rat cuneate nucleus. J Comp Neurol 282:142–156

Wenthold RJ, Hunter C (1990) Immunocytochemistry of glycine and glycine receptors in the central auditory system. In: Ottersen OP, Storm-Mathisen J (eds) Glycine neurotransmission. Wiley, Chichester, pp 391–416

Wenthold RJ, Zempel JM, Parakkal MH, Reeks KA, Altschuler RA (1986) Immunocytochemical localization of GABA in the cochlear nucleus of the guinea pig. Brain Res 380:7–18

Wenthold RJ, Huie D, Altschuler RA, Reeks KA (1987) Glycine immunoreactivity localized in the cochlear nucleus and superior olivary complex. Neuroscience 22:897–912

Wickesberg RE, Oertel D (1988) Tonotopic projection from the dorsal to the anteroventral cochlear nucleus of mice. J Comp Neurol 268:389–399

Wouterlood FG, Mugnaini E (1984) Cartwheel neurons of the dorsal cochlear nucleus. A Golgi-electron microscopic study in the rat. J Comp Neurol 227:136–157

Wouterlood FG, Mugnaini E, Osen KK, Dahl A-L (1984) Stellate neurons in the dorsal cochlear nucleus of the rat studied with Golgi-impregnation electron microscopy; synaptic connections and mutual coupling by gap junctions. J Neurocytol 13:639–664

Young ED (1984) Response characteristics of neurons in the cochlear nuclei. In: Berlin C (ed) Hearing science. College Hill Press, San Diego, pp 423–460

Young ED, Brownell WE (1976) Responses to tones and noise of single cells in dorsal cochlear nucleus of unanesthetized cats. J Neurophysiol 39:282–300

Ziai R, Pan Y-CE, Hulmes JD, Sangameswaran L, Morgan JI (1986) Isolation, sequence, and developmental profile of a brain-specific polypeptide, PEP-19. Proc Natl Acad Sci USA 83:8420–8423

Ziai MR, Sangameswaran L, Hempstead JL, Danho W, Morgan JI (1988) An immunochemical analysis of the distribution of a brain-specific polypeptide, PEP-19. J Neurochem 51:1771–1776